Available online at www.sciencedirect.com
SCIENCE DIRECT®
Plant Science 168 (2005) 635–652
PLANT SCIENCE
www.elsevier.com/locate/plantsci

Compartmentalization of the plant peroxin, AtPex10p, within subdomain(s) of ER☆

Charles Robert Flynn[a,3], Michael Heinze[b,1,3], Uwe Schumann[c,2], Christine Gietl[c], Richard N. Trelease[b,*]

[a]*Arizona State University, Harrington Department of Bioengineering, Arizona Biodesign Institute, POB 879709, Tempe, AZ 85287-9709, USA*
[b]*Arizona State University, School of Life Science, POB 874501, Tempe, AZ 85287-4501, USA*
[c]*Technische Universität München, Lehrstuhl für Botanik, Munich, Germany*

Received 6 August 2004; received in revised form 20 September 2004; accepted 20 September 2004
Available online 21 October 2004

Abstract

A family of proteins collectively referred to as ''peroxins'' are involved variously in the biogenesis of peroxisomes. Recent studies on the characterization of a T-DNA mutant of a putative plant peroxin gene in Arabidopsis, *AtPEX10*, led to conclusions that the peroxin gene product, AtPex10p, is required for normal embryo development and viability, possibly through its involvement in the formation of protein bodies, oleosomes, and peroxisomes from segments of ER. Because the homozygous condition was lethal during seed embryogenesis, Arabidopsis suspension cells were used in the current study for determining the subcellular localization of AtPex10p. Surprisingly, endogenous AtPex10p was not found via immunofluorescence microscopy in peroxisomes; instead, it was observed throughout non-vacuolar cytoplasm partially colocalized with ER marker proteins. Transiently overexpressed AtPex10p (epitope-tagged and fluorescent protein-fused) did not sort to peroxisomes or ER; all constructs accumulated in non-organellar cytosol. Electron immunogold microscopy of the suspension cells confirmed the ER, but not peroxisomal, localization of AtPex10p. Additional evidence for ER localization was obtained from cell fractionation studies. AtPex10p was found exclusively in calnexin-enriched (ER), not catalase-enriched (peroxisomal), regions of sucrose-density gradients. Also, microsomal calnexin and AtPex10p exhibited concomitant magnesium shifts in sucrose gradients, characteristic of localization in rough ER-derived vesicles. AtPex10p in these vesicles was KCl insoluble, alkaline-carbonate soluble, and protease-digestible in the absence of detergent. Collective results indicate that AtPex10p is a cytosolic-facing, peripherally associated membrane protein that occurs in relatively low abundance within portion(s) (subdomains) of ER and possibly in vesicles where it participates in peroxisome formation as an ''early peroxin''.

Keywords: Peroxins; AtPex10p; Endoplasmic reticulum; Organelle biogenesis; Microsomes

1. Introduction

Peroxisomes are unique in their plasticity for conducting a vast array of oxidative, biosynthetic, and degradative metabolic reactions. These single membrane bound organelles do not possess DNA or protein synthesizing machinery, thus they are dependent upon nuclear genes for their protein content. Emanuelsson et al. [18] reported that the proteome for plant peroxisomes is substantially larger than the peroxisomal proteome of any other organisms. This is consistent with the greater number of varied types of plant peroxisomes, e.g., glyoxysomes, leaf (type) peroxisomes, gerontosomes, unspecialized peroxisomes, and other differentiated peroxisomes not specially named but replete with specialized proteins (enzymes) [25,54,51]. Besides the well-characterized pathways of

☆ This work was supported by the National Science Foundation (grant no. MCB-0091826 to RNT) and in part by the William N. and Myriam Pennington Foundation.
* Corresponding author. Tel.: +1 480 965 2669; fax: +1 480 965 6899.
E-mail address: trelease.dick@asu.edu (R.N. Trelease).
[1] Present address: Rote Wand 36, D-32457 Porta Westfalica, Germany.
[2] Present address: Department of Botany, University of Guelph, Ont., Canada N1G 2W1.
[3] These authors contributed equally to this work.

0168-9452/$ – see front matter © 2004 Elsevier Ireland Ltd. All rights reserved.
doi:10.1016/j.plantsci.2004.09.030

photorespiration, fatty acid β-oxidation, glyoxylate cycle, and ureide synthesis [8,50,56,57,75], plant peroxisomes also participate in biosynthesis of plant hormones [67,60] the osmoprotectant glycinebetaine [49], and in valine catabolism [78]. In addition, peroxisomes play essential roles in metabolism of, and thus protection from, reactive oxygen species produced during normal and/or varied stress conditions (e.g., [3,38,12,55]). Recently, peroxisomes have been found to produce signal molecules such as nitric oxide [9,13,73].

Peroxisomal acquisition of these protein repertoires occurs via posttranslational import of membrane and matrix proteins synthesized in the cytosol on unbound polysomes. Matrix proteins are directed to peroxisomes via one of two types of molecular peroxisomal targeting signals, namely PTS1 (a C-terminal tripeptide) or PTS2 (a nonapeptide at the N terminus of proteins) [68]. From analyses of Arabidopsis database searches, Kamada et al. [29] and Reumann [57] independently concluded that about two-thirds of matrix-targeted proteins are PTS1-bearing proteins. Peroxisomal membrane proteins (PMPs) are targeted via a third, distinctly different type of molecular targeting signal, variously designated as a PTS3 or mPTS. This signal generally is composed of transmembrane domain(s) flanked on either side by a cluster of basic amino acid residues described initially for PMP47 in *Saccharomyces* [16], and recently defined in different portions of three different plant PMPs, namely ascorbate peroxidase (APX) [47], PMP22 [48], and Arabidopsis peroxin 3 (AtPex3p) [26].

Proteins that mediate targeting, sorting, and/or uptake of cargo proteins are centrally involved in peroxisomal biogenesis and differentiation [46,74]. Such proteins are collectively named in a numerical order as peroxins (abbreviated Pex) and their genes are abbreviated as *PEX* [15]. In yeasts and mammals, respectively, 32 and 15 *PEX* genes have been identified [21,76], whereas in plants 15 putative Arabidopsis peroxin homologs were identified recently [44,6], but at least 22 peroxin homologs are now known (http://lsweb.la.asu.edu/rtrelease).

Both general and detailed mechanisms of peroxisomal biogenesis (differentiation and proliferation in number) have been debated for many years. In particular, the involvement of ER has been a controversial topic. A so-called ER-vesiculation model described co-translational acquisitions of peroxisomal membrane and matrix proteins into rough ER followed by vesiculation of nascent peroxisomes possessing these acquired proteins from smooth-surfaced subdomains of this ER (reviewed in [30]). This model lost favor due to compelling evidence that peroxisomes could proliferate by growth and division (or division and growth) of pre-existing peroxisomes [33]. Specifying posttranslational acquisition of proteins in this model was a major advance. Research aimed at determining function(s) of peroxins discovered initially in mutant yeasts led once again to models depicting involvement of ER, with the main difference being that proteins were not co-translationally added to ER. Examples of studies providing support for this general model include observations of de novo peroxisomal biogenesis in the ER-rich peripheral region of the yeast *Yarrowia lipolytica*, and findings that the peroxins YlPex2p and YlPex16p were *N*-glycosylated [17,71,2]. Other research with yeasts and plants show that peroxisomal membrane proteins reside in and/or sort through the ER (e.g., [1,59,45,44,30,72,19,36,37]). Indeed, electron microscopic images from a wide variety of plant cells have revealed close associations between peroxisomes and ER (see examples in [74]). The most recent persuasive evidence for ER involvement in peroxisomal biogenesis comes from direct membrane continuities observed between smooth ER ''lamella'' and the peroxisomal boundary membrane elucidated in 3D electron tomographic reconstructions of cryofixed mouse dendritic cells [69,22]. The published model indicates that select membrane peroxin(s) enter rough ER and contribute to formation of specialized extensions of smooth-surfaced ER, which give rise to nascent peroxisomes. These profound results with mouse cells are particularly interesting in view of the lack of any ER involvement in mammalian cell peroxisomal biogenesis reported by others (e.g., [64,32]).

Arabidopsis thaliana PEX10 (*AtPEX10*) was one of the first putative plant peroxin homologs to be isolated [61]. AtPex10p shares 35% amino acid identity with Pex10p homologs in humans (HsPex10p), and with the yeasts *Hansenula polymorpha* (HpPex10p) and *Y. lipolytica* (YlPex10p) [62,66]. All Pex10 homologs, including AtPex10p, contain a RING (C_3HC_4) zinc-binding domain in the C-terminal region [28,53,52], and a signature peptide (-TLGEEY-) in the N-terminal portion of the polypeptide. The former domain has been shown to be necessary for Pex10p function in yeast and mammals, whereas the signature peptide is only presumed to be necessary. In humans, Pex10p dysfunction leads to severe Zellweger syndrome and infantile Refsum disease [53,77].

Several lines of evidence assign multiple roles to Pex10p in peroxisomal matrix protein import. In the absence of functional HsPex10p within human fibroblasts, [4] reported that peroxisomal abundance was reduced five-fold and that matrix proteins were mislocalized to the cytosol. However, peroxisomal ''ghosts'', i.e., membrane vesicles without a full complement of membrane or matrix proteins, were identified in the cells via immunofluorescence with anti-PMP70 IgGs. These peroxisomal ghosts proliferated in number without Pex10p in response to transient expression of Pex11p, a known peroxisomal proliferator. Consequently, it was interpreted that the reduction in peroxisome number was an indirect result of a general defect in peroxisomal matrix protein import. Others showed that loss of the PpPex10p resulted in the accumulation of membrane sheets and vesicles within cytosolic strips that invaginated into the yeast vacuoles [28]. Because these membrane sheets proliferated in response to addition of oleate to the medium, the authors concluded that PpPex10p was not responsible for

peroxisomal proliferation, but likely was responsible for ''peroxisomal lumen formation''. These results indirectly suggest a role for Pex10p in matrix protein import. These findings contrast those describing a *HpPEX10* mutant that lacked any detectable peroxisomal ghosts, but had peroxisomal matrix proteins in the cytosol [70]. Transient overexpression of HpPex10p in these cells resulted in a dramatic increase in nascent small peroxisomes containing HpPex10p leading [70] to conclude that HpPex10p was involved in peroxisome proliferation. Additionally, a role for Pex10p in events following matrix protein import was inferred from interactions of yeast and human Pex10p with other peroxins such as Pex5p, Pex12p, Pex2p, and Pex19p [52,5,63].

Recently, two independent studies of an Arabidopsis Ds insertion mutant defective in Pex10p function were reported [62,66]. Both groups found that seeds homozygous for the transposon disrupting the fourth exon of the *AtPEX10* gene were lethal at the heart stage of embryogenesis. In an ultrastructural study of meristematic cells in a heart-stage embryo, Schumann et al. [62] described extensive defects in the formation of lipid and protein bodies and abnormal morphology of rough ER; peroxisomes were not observed in any of the cells. Interestingly, lipid body monolayer membranes, presumably derived from the bilayer membrane of the ER, accumulated in the cytosol and resembled structures described in the *YlPEX10* mutant. From these observations, Schumann et al. [62] suggest that AtPex10p is directly or indirectly involved in the formation of lipid bodies, protein bodies, and peroxisomes, all three of which have been described in various manners to be related to biogenesis mechanisms involving ER vesicles. However, direct evidence for the existence of AtPex10p in peroxisomes of mutant or wild-type Arabidopsis plants was not reported. Sparkes et al. [66] agreed that AtPex10p is required for normal Arabidopsis embryo development and viability, but they also were not able to provide direct evidence for the occurrence or function of AtPex10p in peroxisomes in the mutant Arabidopsis plants. Instead, they showed in epidermal cells of tobacco leaves a co-localization in peroxisomes of transiently expressed AtPex10p-YFP (yellow fluorescent protein) with transiently expressed GFP-SKL (peroxisomal marker). Certainly, these data contribute to the notion that AtPex10p is a plant peroxin homolog.

In the current study, we describe our combined in vivo and in vitro findings related to the intracellular sorting and subcellular localization of AtPex10p in suspension-cultured Arabidopsis cells. Immunofluorescence microscopy and semi-quantitative immunogold electron microscopy coupled with decisive cell fractionation experiments collectively documented localization of endogenous AtPex10p to rough ER, but not within peroxisomes in these wild-type cells. Integration of findings and interpretations in the literature with our data strongly implicate AtPex10p as an 'early' peroxin homolog that functions in the ER, not in peroxisomes, in some aspect of plant peroxisomal biogenesis.

2. Materials and methods

2.1. Chemicals

Molecular biology reagents were purchased from Promega Corp. (Madison, WI, USA), Qiagen Corp. (Valencia, CA, USA), or New England Biolabs (Beverly, MA, USA). Dithiothreitol (DTT), ethylenediamine tetraacetate (EDTA), HEPES, magnesium chloride, MES, PIPES, β-mercaptoethanol, Trizma base, trichloroacetic acid (TCA), Triton X-100, Tween-20, and Protein A-gold (10 nm) were purchased from Sigma Chemical Co. (St. Louis, MO). Sodium dodecylsulfate was purchased from Serva (Heidelberg, Germany). Sucrose, uranyl acetate, lead citrate, and sodium cacodylate were obtained from J.T. Baker Chemical Co. (Phillipsburg, NJ, USA). Paraformaldehyde and Epon and Spurr's resins were purchased from Ted Pella Inc., (Redding, CA, USA). LR White resin, glutaraldehyde (10% (v/v) aqueous) and osmium tetroxide (4% (v/v) aqueous) were purchased from Electron Microscopy Sciences (Fort Washington, PA, USA).

2.2. Plasmid descriptions and construction

DNA mutagenesis was performed using PCR-based site-directed mutagenesis as described previously [20]. Custom synthetic oligonucleotides for PCR were synthesized by Genetech Biosciences (Tempe, AZ, USA). Base sequences of all mutant DNAs were confirmed by nucleotide sequence analyses performed with an Applied Biosystems 377 automated sequencer at the Arizona State University DNA Laboratory (Tempe, AZ, USA).

Plasmids encoding variants of AtPEX10 were constructed as follows. First, the *Sma*I/*Bam*HI fragment of pZL1/AtPEX10 [61] containing the entire open reading frame (ORF) of AtPEX10 and portions of the 5′ and 3′ untranslated regions (UTRs), was cloned into *Sma*I/*Bam*HI pRTL2ΔNS [34] yielding pRTL2ΔNS/AtPEX10. To generate pRTL2ΔNS/AtPEX10-HA, a non-mutagenic forward primer complimentary to an internal *Bgl*II site within AtPex10 (RF1, Table 1) and a reverse mutagenic primer mutating the stop codon to an *Xba*I site (RF2) were used in a PCR reaction with pRTL2ΔNS/AtPEX10 plasmid DNA as template. The resulting fragment was TA-cloned into pCR2.1 yielding pCR2.1/AtPEX10-*Xba*I. The *Bgl*II–*Xba*I fragment containing the modified 3′-end of AtPEX10 was liberated from pRC2.1 with *Bgl*II and *Xba*I and ligated with *Bgl*II–*Xba*I-digested pRTL2ΔNS/AtPEX10 yielding pRTL2ΔNS/AtPEX10-*Xba*I. Annealed and 5′-phosphorylated oligonucleotides encoding the HA epitope (MYPYDVPDYA) and a stop codon (RF3 and RF4) were

Table 1
Synthetic DNA primers used to generate plasmid constructs used in this study

Primer	DNA sequence
RF1	5′-CCACTCACCAAGAATGATAGATCTTCCATCTTCATCT-3′
RF2	5′-GTTGATCCCATTGTCTAGAAAAATCAGAATGATACAAA-3′
RF3	5′-CTAGATACCCTTACGACGTCCCAGACTACGCTTAGT-3′
RF4	5′-CTAGACTAAGCGTAGTCTGGGACGTCGTAAGGGTAT-3′
RF5	5′-AGATGAAGATGGAAGATCTATCATTCTTGGTGAGTGG-3′
RF6	5′-CCGGTACCGGATCCAGGCTTAATGGGGATTCGGGTCCGGGTCAGGATGAA-3′
RF7	5′-GATCCATGTACCCTTACGACUGTCCCAGACTACGCTC-3′
RF8	5′-GATCGAGCGTAGTCTGGGACGTCGTAAGGGTACATG-3′
RF9	5′-CCGTTACTAGTGGATCTAGATTATTTGTATAGTTCATCC-3′
RF10	5′-CCGTTACTAGTGGATCTAGATTTGTATAGTTCATCC-3′
RF11	5′-AAGGATCCATGAGGCTTAATGGGGATTCGGGTCCGGG-3′
RF12	5′-TCTTTGTTGATCCCATTGGGATCCAAAATCAGAATGATAC-3′
RF13	5′-CATGGAACAAAAGTTGATTTCTGAAGAAGATCTGGGATCCT-3′
RF14	5′-CTAAGGATCCCAGATCTTCTTCAGAAATCAACTTTTGTTC-3′
RF15	5′-AAACCATGGGGCTTAATGGGGATCAGAATGATACAAACA-3′
RF16	5′-TGGGGATCCAAAATCAGAATGATACAAACA-3′

ligated with *Xba*I-digested pRTL2ΔNS/AtPEX10-*Xba*I yielding pRTL2ΔNS/AtPEX10-HA.

To generate pRTL2ΔNS/HA-AtPEX10, PCR mixtures were assembled that included pRTL2ΔNS/AtPEX10 as template DNA, a reverse mutagenic primer (RF5) corresponding to a 19 bp region downstream of a unique *Bgl*II site within AtPEX10, and a forward mutagenic primer (RF6) that replaced the translation initiation site with *Kpn*I and *Bam*HI restriction sites. The resulting PCR product was digested with *Kpn*I and *Bgl*II and ligated with pRTL2ΔNS/AtPEX10 yielding pRTL2ΔNS/*Bam*HI-AtPEX10. *Bam*HI-digested pRTL2ΔNS/*Bam*HI-AtPEX10 was ligated with annealed, kinased double-stranded oligonucleotides (RF7 and RF8) possessing *Bam*HI-compatible ends and coding for a single copy of the HA epitope yielding pRTL2ΔNS/HA-AtPEX10.

For construction of pRTL2ΔNS/GFP and pRTL2ΔNS/GFP-AtPEX10, a portion of pCDNA/GFPS65T (provided by Jim Haseloff, MRC, Cambridge) containing sequences coding for a variant of GFP [23] was amplified by PCR with a forward T7 primer (corresponding to sequences upstream of the GFP initiation methionine) (Promega Corp.) and a reverse primer (RF9 for pRTL2ΔNS/GFP or RF10 for pRTL2ΔNS/GFP-AtPEX10) that either introduced a *Xba*I restriction site downstream of the termination codon (GFP) or replaced the GFP termination codon and a portion of the 3′ UTR with an in-frame *Xba*I site (GFP-*Xba*I). The resulting PCR DNA products were TA cloned into pCR2.1, digested with *Bam*HI, and then ligated into *Bam*HI-digested pRTL2ΔNS [34] to yield pRTL2ΔNS/GFP and pRTL2ΔNS/GFP-*Xba*I. Next, a PCR mixture was assembled that included pRTL2ΔNS/AtPEX10 as template DNA, a reverse non-mutagenic primer (35SRP) and a forward mutagenic primer (RF14) that replaced sequences upstream of the start methionine with an *Xba*I restriction site. The resulting PCR product was TA cloned into pCR2.1, digested with *Xba*I and the *Xba*I-fragment of pCR2.1/*Xba*I-AtPEX10 containing the modified ORF of AtPEX10 was ligated into *Xba*I-digested pRTL2ΔNS/GFP-*Xba*I yielding pRTL2ΔNS/GFP-AtPEX10.

To generate pRTL2ΔNS/AtPex10-GFP, the AtPEX10 ORF was PCR-amplified from pRTL2ΔNS/AtPEX10 using a forward and reverse mutagenic primer set (RF11 and RF12) that introduced *Bam*HI sites upstream of the initiation methionine and in place of the stop codon. The PCR product was digested with *Bam*HI and ligated into *Bam*HI-digested pRTL2ΔNS/GFP [37] yielding pRTL2ΔNS/AtPex10-GFP.

pRTL2ΔNS/*myc*-AtPEX10 was generated by ligating the AtPEX10-containing *Bam*HI-fragment from pRTL2ΔNS/*Bam*HI-AtPEX10 with *Bam*HI-digested pRTL2ΔNS/*myc*–*Bam*HI–*Xba*I (kindly generated by Dr. Robert Mullen) yielding pRTL2ΔNS/*myc*-AtPEX10. The plasmid pRTL2ΔNS/*myc*–*Bam*HI–*Xba*I was constructed by ligating two annealed synthetic oligonucleotides (RF13 and RF14) coding for the *myc* epitope plus the initiation methionine and *Nco*I–*Xba*I complementary ends into *Nco*I–*Xba*I-digested pRTL2.

pCAMBIA/AtPEX10-YFP was provided by Sparkes et al. [66], who in the final preparation step inserted the fragment 35S-AtPEX10-eYFP-NOS into the binary vector pCAMBIA 1300. This DNA was used as such for biolistic bombardment of Arabidopsis and BY-2 suspension cells.

2.3. Preparation of rabbit anti-Arabidopsis Pex10p (AtPex10p) antiserum

AtPEX10 was subcloned into *Nco*I and *Bam*HI restriction sites of the pQE60 expression vector (Qiagen, Valencia, CA, USA) with an added extension coding for 6xHis [62]. These sites were added to the 5′ and 3′ end of AtPEX10 using the sense primer (RF15, Table 1) and anti-sense primer (RF16). AtPex10p-6xHis was overexpressed in *E. coli* (M15) and affinity-purified by Ni-affinity chromatography (Qiagen, Valencia, CA). AtPex10p-6xHis, eluted from the column in 8 M urea, was diluted to 2 M urea, 150 mM NaCl and 0.1% Triton X-100 (pH 7.5–8.0), and then concentrated with

Centriplus 30 microconcentrators (Millipore Inc.) to 0.8 mg/mL. Rabbit antiserum was prepared commercially by Davids Biotechnology, Regensburg, Germany. IgGs were affinity purified via Protein A-Sepharose chromatography according to [31].

2.4. Cell culture, microprojectile bombardment, and (immuno)fluorescence microscopy

A. thaliana var. Landsberg erecta suspension-cultured cells were cultured in a Murashige and Skoog salt and vitamin growth medium according to [36]. Cells were harvested 4-day post weekly subculture. Processing of wild-type (non-transformed) and microprojectile-bombarded (transiently transformed) cells for immunofluorescence microscopy was described previously in detail [36]. A modification employed in this study was that formaldehyde-fixed wild-type cells were incubated in 0.1% Pectolyase Y-23 plus 0.05% Cellulase RS instead of 0.1% Pectolyase Y-23 and 0.1% Cellulase RS. This modification improved the morphological appearance of the cells, whether the cells subsequently were processed using our standard 1 mL volume ''tube'' procedure or our ''on-slide'' procedure. For the latter procedure, fixed and perforated/digested (pectolyase/cellulase) cells were adhered to poly-L-lysine-coated microscope slides prior to permeabilization in 0.5% Triton X-100 and incubations in primary and secondary antibodies. Except for Fig. 2, all of the non-confocal images of non-transformed cells presented in this paper were obtained from cells prepared via the ''on-slide'' procedure; the standard tube procedure was not suitable for obtaining images of endogenous AtPex10p (compare Fig. 2A and B). Transient transformations via microprojectile bombardment of cells with GFP-fusion or epitope-tagged-AtPEX10 constructs, and subsequent processing of cells (via the tube procedure), were done as described in [36]. More specifically, bombarded cells held on Petri plates in transformation medium for 5 h were fixed (4% formaldehyde) and perforated/digested with Pectolyase Y-23 and Cellulase RS. Notably, fixation of the cells did not impair the GFP fluorescence signal; hence, fixed and Triton X-100-permeabilized cells usually were labeled also with varied marker primary antibodies and appropriate dye-conjugated secondary antibodies.

Antibody concentrations, incubation times, and sources used for immunofluorescence microscopy were as follows (affinity-purified IgGs were those bound and then eluted from Protein A-Sepharose columns): rabbit anti-Arabidopsis Pex10p affinity-purified IgGs (1:100, 3 h) [62]; rabbit anti-cucumber peroxisomal APX affinity-purified IgGs (1:500, 3 h) [10]; rabbit anti-cottonseed catalase affinity-purified IgGs (1:500, 1 h) [31]; rabbit anti-castor calnexin antiserum (1:500, 1–3 h) (provided by Coughlan et al. [11]); mouse anti-HA epitope monoclonal antibody (1:300, 1 h) (Roche, Basel, Switzerland); mouse anti-c *myc* monoclonal antibody (1:500, 1 h) (9E10, purified, Covance Research Products Inc. Berkeley, CA); mouse anti-salicylic acid-binding protein (catalase) monoclonal antibody (1:250, 1 h) [7]; rabbit anti-pea reversibly glycosylated polypeptide (RGP1) antiserum (1:500, 1 h) (provided by Dhugga et al. [14]); mouse anti-maize β-ATPase E monoclonal antibody (1:10, 1 h) (provided by Elthon and coworkers [40]); anti-mouse Hsc70 (BiP) (1:2000, 30 min) (StressGen Inc., San Diego, CA); rabbit anti-cucumber PMP73 IgGs (1:500, 1 h) [10]; goat anti-rabbit rhodamine (1:1000); goat anti rabbit cyanine (Cy) 2 (1:500); goat anti-rabbit Cy5 (1:500); goat anti-mouse rhodamine (1:500); goat anti-mouse Cy2 (1:500 or 1:1000), goat anti-mouse Cy5 (1:500). All fluorophore-conjugated secondary antibodies, purchased from Jackson ImmunoResearch Laboratories (Westgrove, PA), were incubated with cells for 30 min to 1 h. Concanavalin A conjugated to Alexa 594 (100 μg/mL in PBS, 20 min) was purchased from Molecular Probes (Eugene, OR). Mounting of cells on microscope slides for both non-confocal and confocal laser epifluorescence microscopy via the tube procedure was done as described previously [36]. Non-confocal microscopy was done with a Zeiss Axiovert 100 microscope and confocal laser microscopy was done with a Leica TCS NT microscope. Adobe Photoshop 7.0 (Adobe Systems, Mountain View, CA) was used to enlarge, pseudocolor and assemble the obtained images into figures.

2.5. Differential centrifugations, SDS-PAGE, immunoblot analyses, sucrose-gradient isolation of organelles, and Mg^{2+} shift subfraction of microsomes

Details for most of the methods and procedures listed in the above headings have been described previously [36]. Below, we state the general procedures used in the current study and emphasize all modifications and exceptions.

For differential centrifugations, 7-day-old Arabidopsis cells (25 mL portions) were resuspended in 1.5 volumes of ice-cold homogenization medium (HM) consisting of 25 mM HEPES-KOH, pH 7.5, 3 mM DTT, and 0.5 mM phenylmethylsulfonyl fluoride. Following one passage through a French pressure cell at 4000 psi, this homogenate was centrifuged at 1500 × *g* (20 min) in a Beckman JS-13 rotor at 4 °C, then the supernatant was centrifuged in a Beckman 90 Ti rotor at 200,000 × *g* for 1 h at 4 °C. Aliquots of the homogenate, the 200,000 × *g* pellet (resuspended in HM), the 200,000 × *g* supernatant, and selected sucrose-density gradient (30–59% (w/w) Suc—Fig. 6, 15–45% (w/w) Suc—Fig. 7) fractions were taken to a final concentration of 0.05% (w/v) deoxycholate (Sigma), incubated for 15 min (room temperature), added to an equal volume of 20% (w/v) TCA, incubated for 30 min (4 °C), and then centrifuged in 1.5 mL microfuge tubes at about 10,000 × *g* for 15 min (4 °C). TCA precipitates were resuspended in SDS sample buffer containing 5 mM DTT, neutralized with solid Tris, boiled for 15 min, and then polypeptides were separated in 12% (w/v) precast Mini-Protean II polyacrylamide gels (Bio-Rad). Amounts of protein in samples shown in Fig. 1

(lanes E–G) were determined using the standard bicinchonic acid (BCA) protocol with BSA as the standard (PIERCE, Rockford, IL), whereas protein amounts in all other samples were determined using the standard Coomassie Blue dye-binding assay with plasma gamma globulin as the standard (Bio-Rad). Electroblotting and immunodetections of antigens on PVDF membranes using the ImmunStar chemiluminescence kit were the same as described. Rabbit anti-Arabidopsis Pex10p antiserum and rabbit anti-castor calnexin antiserum were applied at 1:1000 and 1:5000 dilutions, respectively. Ni-alkaline phosphatase was used to directly detect the polyhistidine tag on proteins within the gel. Organelle isolations in sucrose gradients (Fig. 6), Mg^{2+} shift experiments (Fig. 7), and membrane association/topological orientation procedures with rough microsomal vesicles (Fig. 9) were done as described by Lisenbee et al. [36], except the methods for SDS/PAGE, protein determination, detergent (deoxycholate) solubilization of proteins, and TCA precipitation of proteins were done as described above.

2.6. Electron microscopy and immunogold labeling

Detailed ultrastructural observations of Arabidopsis suspension-cultured cells were acquired from ultrathin sections of cells prepared according to the methods used for BY-2 cells described by Sabba et al. [58], with the following modifications. All preparative steps with the Arabidopsis cells were performed at room temperature on a clinical rotary inverter unless otherwise indicated. One milliliter of 6% glutaraldehyde in 50 mM PIPES-NaOH, pH 7.4, was added to a 10 mL portion of 4-day post-subculture Arabidopsis cells maintained under constant rotary gyration. After 2–3 min, cells were removed from the gyrator and maintained in the fixative solution for 1 h. A 2 mL aliquot of the fixed cells, washed twice in a 100 mM cacodylate buffer, pH 7.4, was post-fixed for 2 h in 2% (v/v) osmium tetroxide in the same buffer. After washes in deionized water and incubation in 2% (w/v) aqueous uranyl acetate for 2 h, cells were dehydrated in a graded series of ethanol and infiltrated in a graded series of 50% Epon/50% Spurr's resins. Cells transferred to tapered BEEM (Ted Pella Inc. trade name) capsules were pelleted in a microcentrifuge at about 13,000 × *g* for 5 min prior to polymerization at 68 °C for 40 h. Silver–gold sections (about 70 nm) were cut with a diamond knife, mounted on copper grids, and post-stained with 2% (w/v) aqueous (50%) uranyl acetate for 10 min and then Reynold's lead citrate for 5 min.

For immunogold labeling of intact cells, Arabidopsis cells were fixed as described above in a final concentration of 0.6% glutaraldehyde, but not post-fixed in osmium tetroxide. Following washes in cacodylate buffer and deionized water, cells were dehydrated in a series of ethanol and then infiltrated with LR White resin. Embedded cells were transferred to tapered BEEM capsules and then pelleted in a microcentrifuge at about 13,000 × *g* for 5 min prior to polymerization at 50 °C for 24–48 h under vacuum.

Microsomal subfractions collected from sucrose gradients that were prepared for immunogold electron microscopy were fixed in 0.75% (v/v) glutaraldehyde in *iso*-osmotic sucrose in 25 mM HEPES-KOH, 5 mM $MgCl_2$, pH 7.5, without osmication, and embedded in LR White resin as described in detail by Lisenbee et al. [36]. Gold ultrathin sections (about 90 nm) of cells and subfractions were collected on formvar-coated nickel grids.

The same immunogold-labeling procedures and conditions were employed for sections of Arabidopsis cells and microsomal subfractions. Sections were pretreated for 30 min in 1.0% (w/v) glycine and blocked for 30 min in 1% (w/v) BSA in PBS. More details of the immunogold-labeling procedure are given in [36]. Sections were floated for 3 h on drops of primary antibodies (preimmune antisera or Protein A-affinity-purified IgGs of anti-Arabidopsis Pex10p, anti-cucumber peroxisomal APX, or anti-castor calnexin antiserum) diluted 1:50 in blocking solution (1% BSA in PBS and 0.01% sodium azide). After extensive washes in PBS, the grids were floated for 45 min on 10 nm gold-conjugated Protein A diluted 1:25 in blocking solution. Following 3–4 washes in PBS and deionized water, grids were post stained for 5 min in aqueous uranyl acetate and 1 min in lead citrate. Digital images of all of the above samples were obtained with a Gatan Slow Scan Camera (Type 694) connected to a Philips CM12S transmission electron microscope (operated at 60 or 80 kV) and were processed with DigitalMicrograph software, version 3.7.4 (Gatan Inc., Pleasanton, CA). Unaided eye observations were used to count the number of gold particles over sectioned rough microsomal vesicles in LR White sections of the 42% sucrose gradient fractions (Fig. 8). Numbers of gold particles were obtained from at least five prints on glossy paper (most data from eight prints) that were made from the digital images with the electron microscope. Values were normalized per μm^2 of the material in the sectioned gradient fractions to obtain comparative gold particle counts. Gold particles/μm^2 were not counted in glossy prints of sections through Arabidopsis cells (e.g., Fig. 5) because comparative data among prints (of digital images) would not be reliable due to non-uniform areas of the sections that contain variable views of different organelles in the sections. Instead, representative images of 15–20 digital electron micrographs were selected for each applied antibody experiment and are presented in Fig. 5.

2.7. Distribution of materials

Upon request, all novel materials described in this publication will be made available in a timely manner for non-commercial research purposes, subject to the requisite permission from any third-party owners of all or parts of the material. Obtaining any permissions will be the responsibility of the requestor.

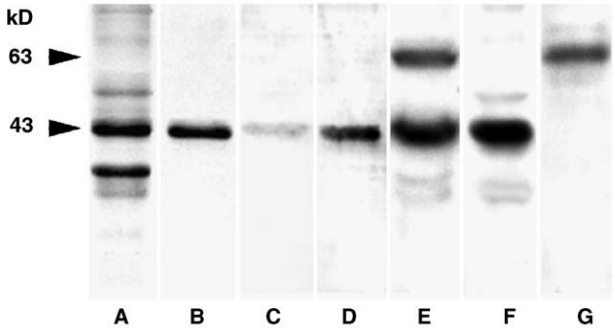

Fig. 1. Rabbit anti-Arabidopsis Pex10p (AtPex10p) Protein-A-purified IgGs selectively recognize a major 43 kD polypeptide in microsomal pellets that were derived from Arabidopsis suspension cell homogenates. Lanes A–D are from SDS polyacrylamide gels and lanes E–G are PVDF (Immobilon) membrane electroblots. Inclusion bodies isolated from *E. coli* cells over-expressing AtPex10p-6xHis possessed a major Coomassie Brilliant Blue-stained 43 kD polypeptide band (lane A) that was recognized by the Ni-alkaline phosphatase probe (lane C). AtPex10p-6xHis antigen, which was affinity purified from inclusion body extracts via Ni-NTA affinity-chromatography, was composed of only one Coomassie-blue-stained 43 kD polypeptide band stained with Coomassie Blue (lane B) and was identified as such with the Ni-alkaline phosphatase probe (lane D). IgGs, affinity purified from the rabbit AtPex10p antiserum, recognized on blots of Arabidopsis clarified homogenates (lane E) a major 43 kD band and another less prominent band 63–66 kD band. The most prominent band in the microsomal pellet (200,000 × *g*, 1 h) (lane F) was a 43 kD polypeptide band, which was absent from the supernatant that exhibited only 63–66 kD polypeptide band (lane G). Lanes A–D, 10 μg protein; lanes E–G, 150 μg protein per gel lane.

3. Results

3.1. Characterization of AtPex10p antigen and rabbit AtPex10p antiserum

Rabbit antibodies were raised against affinity-purified, his-tagged AtPex10p overexpressed in *E. coli* from *AtPEX10* cDNA isolated by Schumann et al. [61]. The predicted molecular mass of AtPex10p is 42.6 kD. Fig. 1 illustrates selected samples, separated in SDS gels, which are related to the production and characterization of these antibodies. Lane A shows that the inclusion bodies contain prominent Coomassie-blue stained 43 kD polypeptides and lane B shows that only the 43 kD AtPex10-6xHis antigen recovered from the Ni-affinity column is stained with Coomassie blue in the gels. Confirmation of these results and interpretations are shown in lanes C and D where Ni-alkaline phosphatase probes of the inclusion bodies (C) and the purified antigen (D) in gel slices produced reaction products detecting only 43 kD polypeptide in each gel lane.

Sensitive chemiluminescence antibody detections of Arabidopsis suspension cell samples electroblotted to Immobilon reveal a high degree of anti-AtPex10p Protein-A IgG specificity. Fig. 1 (lane E) shows a major, prominent 43 kD polypeptide band (AtPex10p) and a less prominent 63–66 kD band (unidentified polypeptide) in clarified homogenates of Arabidopsis cells. Lane F shows that AtPex10p also was the major polypeptide (43 kD band) recognized in the microsomal pellets recovered from the cell homogenates. These data, the complete absence of these AtPex10p polypeptides in the microsomal supernatants (lane G), and the two predicted transmembrane domains (TMDs) [61,66], collectively indicate that AtPex10p is a membrane-associated protein in Arabidopsis cells. The unidentified 63–66 kD polypeptide in the cell homogenate (lane E) and soluble (supernatant) fraction (lane G) did not hinder interpretations of results of our cell fractionation experiments, including the electron immunogold microscopy, because microsomal pellets did not possess this polypeptide (lane F) and these pellets were the samples applied to the sucrose gradients (see later).

3.2. In vivo immunofluorescence microscopy of endogenous AtPex10p in Arabidopsis suspension cells

Fig. 2 is a grouping of representative immunofluorescence images that illustrates two features: (a) necessary procedures for epifluorescence immuno-detection of native AtPex10p in Arabidopsis suspension cells (panels A–B), and (b) the localization of endogenous AtPex10p in wild-type cells (panels D–O).

Virtually all of our previous immunofluorescence studies (confocal and non-confocal epifluorescence microcopy) with suspension-cultured cells (BY-2 and Arabidopisis) have been done using our standard 1 mL volume procedure. In this procedure, all reagents (including antibodies) are added to cells in a microfuge tube prior to spreading them on a slide for epifluorescence observations (e.g., [20,45,44,26]). This standard procedure with anti-AtPex10p IgGs (Protein-A purified), including numerous reagent variations thereof, was employed to define the subcellular site of endogenous AtPex10p. Fig. 2A illustrates typical results; none of the Arabidopsis cells on the slides exhibited an epifluorescence signal above the baseline autofluorescence signal. Lisenbee et al. [36] experienced similar difficulties when attempting to determine the subcellular localization of endogenous peroxisomal membrane ascorbate peroxidase (APX). A simple, but significant modification of the cell preparation procedure, referred to as the 'on-slide' procedure, resulted in above-background epifluorescence signals attributable to applications of primary and secondary antibodies to cells already affixed to the microscope slides. Fig. 2B illustrates a representative cluster of about 11 Arabidopsis cells, each of which exhibits AtPex10p-dependent cyanine 2 (Cy2) epifluorescence of structures throughout their cytoplasms. A representative result of control experiments done for this immunofluorescence procedure is shown in Fig. 2C, where rabbit preimmune serum (plus Cy2-conjugated secondary antibodies) was applied to the slides in place of anti-AtPex10p IgGs. Only weak autofluorescence of a cluster of cells is observed in Fig. 2C. Similar weak-signal images consistently were observed when other controls were applied, such as omission of primary anti-AtPex10p IgGs

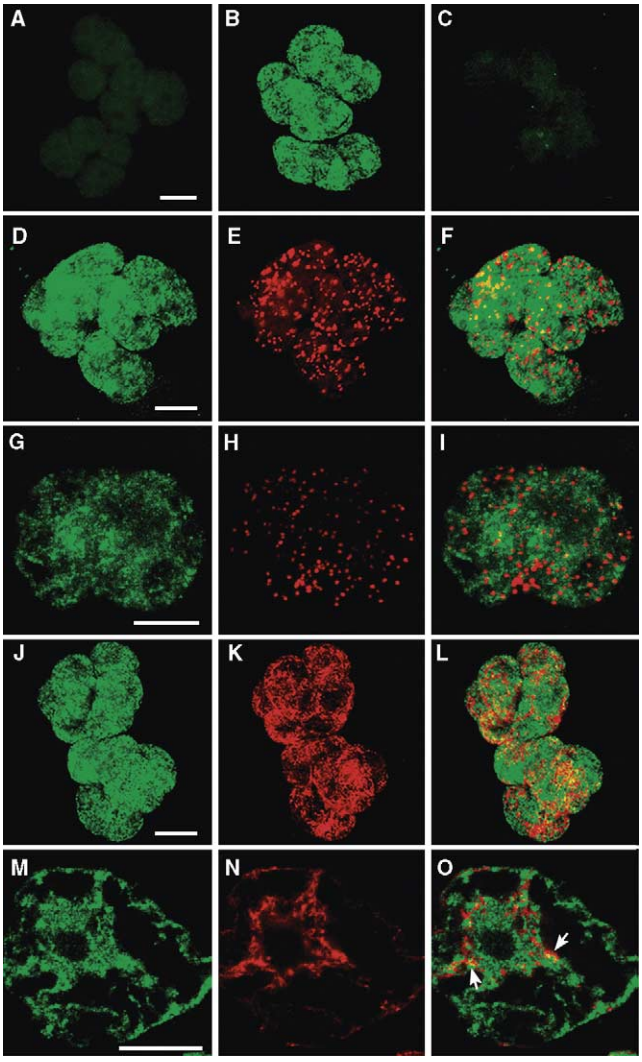

Fig. 2. Immunofluorescence microscopy reveals localization of endogenous AtPex10p with a portion of ER, but not within peroxisomes, in Arabidopsis suspension cells. Cells (4-day subculture) were fixed (formaldehyde), cell walls were perforated and partially digested (pectolyase and cellulase), membranes were permeabilized (Triton X-100), and primary and secondary antibodies were added to cells in a microfuge tube (standard 1 mL procedure), or to cells already affixed to microscope slides (on slide procedure). (A) Cells processed using the standard tube procedure with anti-AtPex10p IgGs (Protein-A affinity purified) and Cy2-conjugated secondary antibodies are barely visible (baseline autofluorescence) (non-confocal microscopy). (B–F) and (J–L) Cells were processed via the on-slide procedure. (B) AtPex10p immunofluorescence (Cy2) is in structures observed throughout the cytoplasm of each of the 11 clustered cells (non-confocal microscopy). (C) An immunofluorescence signal above the background level is not observed in the clustered cells incubated in preimmune serum and Cy2-conjugated antibodies (non-confocal microscopy). (D–F) The same cluster of cells dual labeled with rabbit anti-AtPex10p IgGs and Cy2 (D), mouse anti-catalase monoclonal IgGs and rhodamine (E), a computer merged image (F) (non-confocal microscopy). (G–I) A single cell that is dual labeled as are the cells shown in (D–F) (confocal projection images). (J–L) The same cluster of cells dual labeled with rabbit anti-AtPex10p IgGs and Cy2 (J), mouse anti-BiP monoclonal IgGs and rhodamine (K), a computer merged overlay (L) (non-confocal microscopy). (M–O) A single cell that is dual labeled as the cells shown in (J–L) (confocal slice images). Arrows denote colocalizations. Bars = 5 μm.

(plus secondary antibodies) or substitution of irrelevant antibodies (rabbit IgGs) for anti-AtPex10p IgGs (data not shown). Images for panels A through C were captured using the same exposure time.

It was postulated at the outset of this study that endogenous (native) Atpex10p existed in Arabidopsis peroxisomes (boundary membrane). However, Fig. 2B shows that cells labeled with anti-AtPex10p IgGs do not exhibit a punctate pattern, although AtPex10p-containing peroxisomes could be dispersed among the cytoplasmic-labeled structures. To test this hypothesis, cells were dual-labeled for non-confocal epifluorescence microscopy with rabbit anti-AtPex10p polyclonal IgGs plus mouse anti-catalase monoclonal IgGs (Fig. 2D–F) using the on-slide method. The expected result was a punctate colocalization of catalase and AtPex10p in peroxisomes. Fig. 2D shows a cytoplasmic AtPex10p immunofluorescence pattern within each of the clustered cells (similar to that in Fig. 2B). In the same cluster of cells as those shown in Fig. 2D, a punctate catalase pattern characteristic of peroxisomes is apparent in each cell of the cluster (Fig. 2E). The merged image shown in Fig. 2F shows a mixture of red and yellow peroxisomes, making it difficult to interpret whether AtPex10p and catalase exist together within peroxisomes. Of particular interest, however, are the observations that AtPex10p seemingly exists within some other cytoplasmic structure.

In an attempt to resolve the possible in vivo colocalization of AtPex10p and catalase, these dual labeled cells were examined in greater detail using laser confocal microscopy. Fig. 2G–I illustrates immunofluorescence patterns within the cytoplasms of two cells, rather than a cluster of cells as described above. In Fig. 2G, fluorescence due to AtPex10p is observed transversing all parts of the non-vacuolate cytoplasm. Fig. 2H illustrates anti-catalase immunofluorescence in punctate peroxisomes distributed throughout the cytoplasm; identical punctate AtPex10p fluorescence structures are not observed in Fig. 2G. The merged overlay in Fig. 2I confirms this observation; that is, red, pseudocolorized peroxisomes are distinct from the green AtPex10p fluorescence pattern. This higher resolution image of a single cell is representative of other confocal slice and projection images (not shown) that are interpreted to indicate the in vivo non-colocalization of AtPex10p and peroxisomal catalase.

Fig. 2J–O illustrates results of in vivo dual-labeling experiments aimed at identifying the cytoplasmic site of the observed AtPex10p immunofluorescence, specifically whether AtPex10p exists in ER in these cells. The cluster of cells illustrated in Fig. 2J shows virtually the same AtPex10p immunofluorescence pattern as described above. The same cluster of cells (Fig. 2K) labeled with the anti-BiP ER marker shows structures resembling ER that traverse the cytoplasm of each cell in the cluster. The morphological appearances of the ER and AtPex10p immunofluorescence images are not identical, but certainly are similar. The merged image (Fig. 2I) shows that the AtPex10p and ER BiP

images are not completely super imposable, but areas in each cell elicit a yellow color indicative of a partial colocalization of AtPex10p with ER BiP. A representative laser confocal slice image of one of these dual-labeled cells (Fig. 2M–O) provides greater resolution of the immunofluorescence images. AtPex10p labeled structures transverse the non-vacuolate cytoplasmic strands and are apparent in the perinuclear region of this cell (Fig. 2M). ER BiP images in the same cell also are observed in the cytoplasmic strands and perinuclear region (Fig. 2N). The merged image (Fig. 2O) shows that AtPex10p and ER BiP images are not totally superimposable as in Fig. 2L, but certainly a portion of the ER is colocalized (arrows) with the AtPex10p structures, especially in the perinuclear region. Numerous epifluorescence images examined during the course of this study have shown similar partial colocalizations of these two antibody labels. These observations are interpreted to indicate that a portion of the endogenous AtPex10p exists within select areas or subdomains of the total cellular ER.

3.3. *In vivo immuno- and auto-fluorescence microscopy of transiently expressed AtPex10p fusions in Arabidopsis suspension cells*

The surprising negative results for the existence of AtPex10p in Arabidopsis peroxisomes prompted a series of transient, overexpression experiments. These experiments were designed to test hypotheses that AtPex10p existed in peroxisomes at a low, undetectable steady state level, which may increase to an immunofluorescence-detectable level following transient overexpression of AtPex10p constructs. Overexpression may also increase the level of AtPex10p constructs in the non-peroxisomal compartment (Fig. 2); this result could help elucidate its identity and role in intracellular sorting of AtPex10p.

Fig. 3A is a representative image of the cellular localization of transiently expressed HA-epitope-tagged AtPex10p. The fluorescence is throughout the cytoplasm, not localized within any structure or organelle. Such images are indicative of an accumulation of the expressed protein throughout the cytosol of transformed cells (see Fig. 3C as a positive control expressing GFP alone). This result was not expected. Fig. 3B shows that catalase-containing peroxisomes appear normal in the same transformed cell. This indicated that peroxisomes were not overtly disrupted in response to biolistic bombardment or AtPex10p overexpression and therefore were present to acquire accumulated HA-AtPex10p from the cytosol. Transiently expressed AtPex10p with an N terminal *myc* epitope tag also was observed throughout the cytosol of transformed cells (data not shown). In Fig. 3C, the autofluorescence image of overexpressed GFP throughout the cytosol is shown. Note that this uniform-appearing image and that of HA-AtPex10p (Fig. 3A) are quite distinct from the more structured cytoplasmic, non-confocal images of native AtPex10p shown in Fig. 2B, D, and G. Fig. 3D illustrates the result

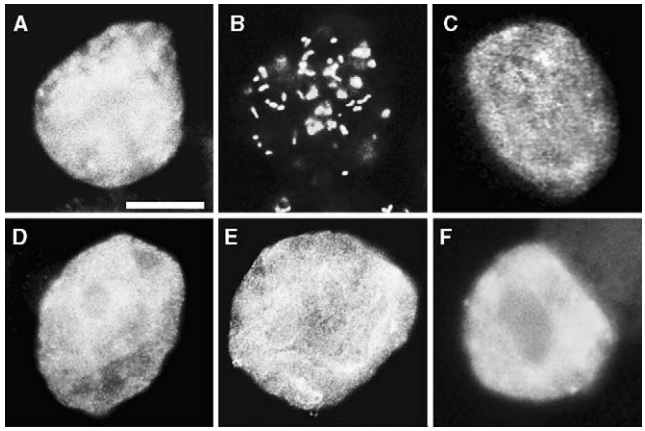

Fig. 3. Transiently expressed AtPex10p that has been epitope tagged, fused to GFP, or fused to YPF accumulates in the cytosol of Arabidopsis suspension cells. (A and B) The same dual immuno-labeled cell showing the cytosolic localization of transiently expressed (5 h post bombardment) HA-AtPex10p (Cy2) (A) and the peroxisomal localization of endogenous catalase (rhodamine) (B). (C) GFP autofluorescence throughout the cytosol of one cell expressing (5 h) GFP. (D) GFP autofluorescence throughout the cytosol of one cell expressing (5 h) GFP-AtPEX10. (E) GFP autofluorescence of one cell expressing (5 h) AtPex10p-GFP. (F) YFP fluorescence throughout the cytosol of a cell expressing (22 h) Pex10-YFP. All cells were fixed in formaldehyde, and all images are non-confocal epifluorescence images. Bar = 5 μm.

of GFP-AtPex10p expression in the cells. This fusion protein also was not sorted to or taken up into any compartment within the cells. The possibility that fusion of GFP to the N terminal end of AtPex10p blocked a peroxisomal targeting signal was addressed by expressing another construct with GFP fused to the C terminus of AtPex10p. Fig. 3E shows that this construct, AtPex10-GFP, also was distributed throughout the cell cytosol. A similar construct with YFP fused at the C terminus shows the same result (Fig. 3F) as that found with GFP bound to the C terminus of AtPex10p (Fig. 3C). The YFP construct is the same one that was transiently expressed in tobacco leaf epidermal cells and reported to localize to the peroxisomes in these cells [66]. All of the GFP and the YFP constructs described above were observed in transformed live cells prior to fixation in formaldehyde and immunolabeling with anti-catalase antibodies to visualize the peroxisomes in the transformed cells. In all cases, the autofluorescence was observed in the cytosol of the live cells, and normal-appearing peroxisomes were observed in the formaldehyde-fixed cells transformed with GFP and YFP AtPex10p constructs (data not shown).

3.4. *Immunogold electron microscopy of AtPex10p in Arabidopsis suspension cells*

Results of the in vivo (immuno)fluorescence experiments above do not support the hypotheses that endogenous AtPex10p exists in peroxisomes, or that overexpressed AtPex10p is acquired by peroxisomes. Instead, it appears that this protein exists in a non-peroxisomal compart-

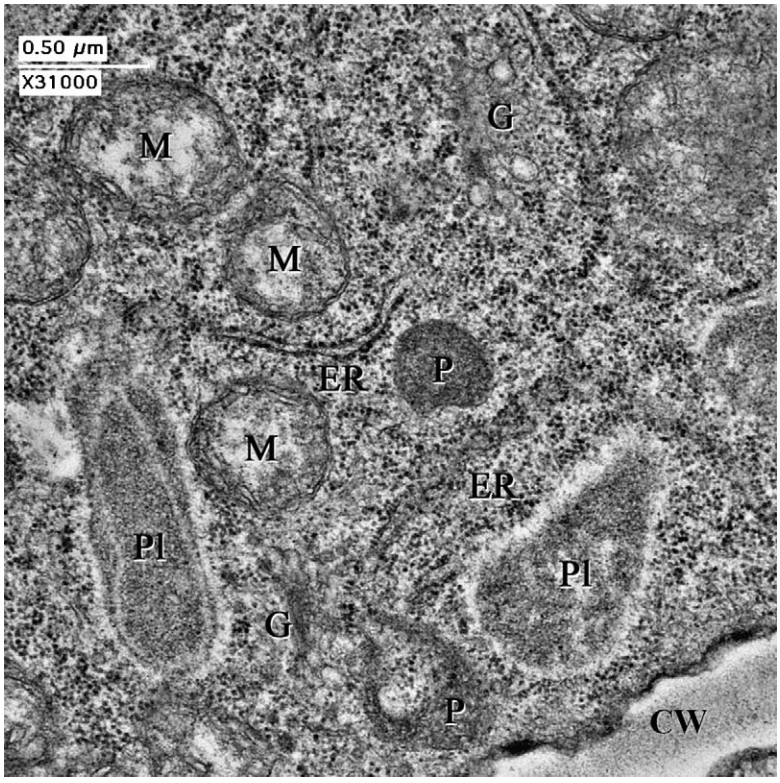

Fig. 4. Rough ER (ER), peroxisomes (P), and other organelles are prevalent in the non-vacuolate portion of the cytoplasm in an Arabidopsis suspension cell fixed in glutaraldehyde and osmium tetroxide and post-stained with uranyl acetate and lead citrate. The representative transmission electron micrograph illustrates abundant rough ER distributed throughout this area of the cytoplasm. Mitochondria (M), non-green plastids (Pl), and Golgi bodies (G) also occur commonly in the cell cytoplasm. Cell wall (CW). Bar = 0.5 μm.

ment(s), seemingly in subdomains of ER. Electron immunogold microscopy of the cells was done to help resolve the subcellular localization(s) of endogenous AtPex10p.

At least 20 digital images of glutaraldehyde/osmium tetroxide-fixed Arabidopsis suspension cells similar to the electron micrograph shown in Fig. 4 were captured and thoroughly examined to help interpret the epifluorescence results described above and the immunogold labeling results presented in Fig. 5. Fig. 4 is a representative micrograph of a thin section through a portion of the non-vacuolate cytoplasm. It shows the common occurrence of mitochondria, Golgi bodies, plastids, peroxisomes and rough ER in this area of the cell. Abundant rough ER is observed in profile and surface views among all of the organelles. Unbound polysomes are numerous and close together in the cytosol among the organelles. The abundance of small, single membrane bound vesicles in the cytoplasm, except those derived from Golgi bodies, is not a special feature of these cells.

Fig. 5 shows representative results of the electron immunogold experiments. Only a small area of the cell sections that were examined is presented in the three panels of the figure. A semi-quantitative assessment of gold labeling, e.g., particle counts per area or organelle, is not presented with these micrographs for reasons described in Section 2. In general, the number of bound gold particles per section area was low, and particles were not concentrated over any organelle in the sections. However, the frequency of gold particle binding due to application of anti-AtPex10p (Fig. 5A) or anti-calnexin (Fig. 5B) antibodies obviously was greater than binding frequency due to application of preimmune serum (Fig. 5C). This is apparent in a visual comparison of the three panels. Given the qualitative nature of these results, gold particle binding attributable to the two antibodies was most prevalent over sectional views of ribosome-studded membrane structures, i.e., segments of rough ER, in the cytoplasm of the cells. A biased visual search on the electron microscope for gold particle binding over peroxisomes or any other organelles such as the one shown in Fig. 5A did not reveal any such labeling. Taken at face value from numerous observations and evaluations of gold particle binding, AtPex10p and calnexin appear to be preferentially localized in rough ER.

3.5. Cell fractionation analyses

Cell fractionation was selected as an alternative approach to elucidate the endogenous subcellular site(s) of AtPex10p in the suspension cells. Intact organelles (except starch-containing plastids and nuclei) in clarified homogenates can be separated within a continuous 30–59% Suc-density

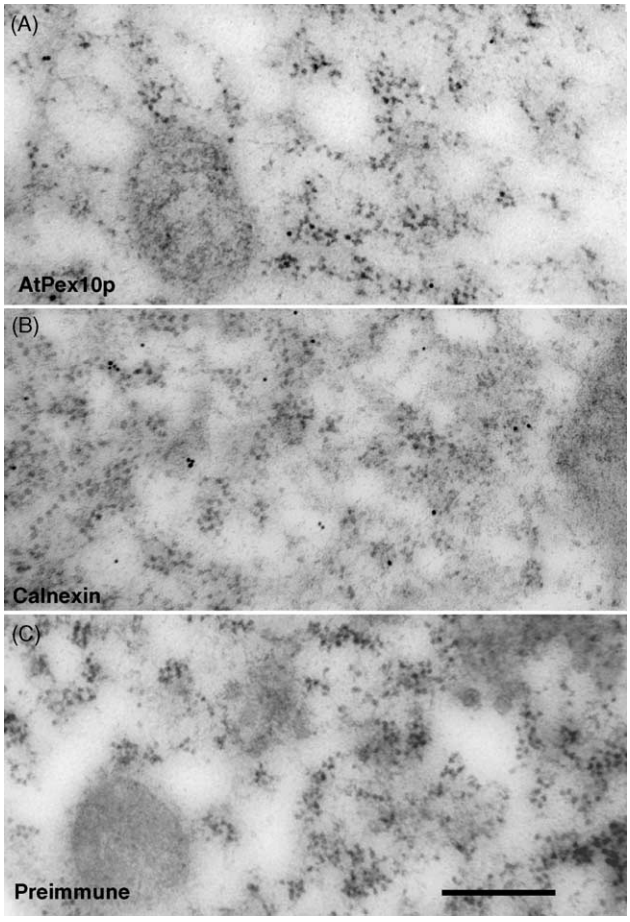

Fig. 5. Electron immunogold microscopy of Arabidopsis cells indicates that endogenous AtPex10p exists in portions of the rough ER. (A) Protein A-gold particles are localized selectively to rough ER profiles in thin sections treated with anti-AtPex10p IgGs. (B) Protein A-gold particles are localized selectively to rough ER profiles in thin sections treated with anti-calnexin antiserum. (C) Protein A-gold particles are observed infrequently at any location on thin sections treated with preimmune serum. Cells were fixed in 0.6% glutaraldehyde (not post-fixed in osmium tetroxide), and LR White sections were post-stained with uranyl acetate and lead citrate. Bar = 0.2 μm.

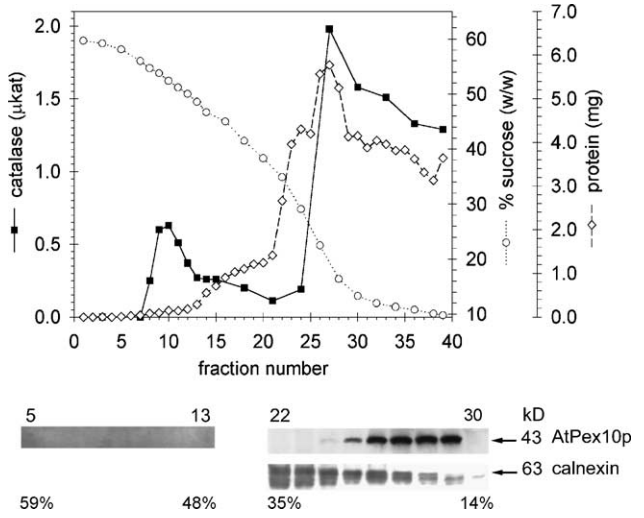

Fig. 6. AtPex10p is immunodetected in Suc density-gradient fractions that also possess immuno-reactive calnexin, but is not detected in fractions with catalase activity (isolated peroxisomes). Approximately 12 mL of a clarified cell homogenate (1500 × *g* supernatant, 15 min, in 13% (w/w) Suc) was layered onto a 25 mL 30–59% (w/w) Suc gradient in a Beckman VTi 50 rotor. After centrifugation, proteins in 1 mL fractions were detergent solubilized (in deoxycholate) and TCA-precipitated for SDS/PAGE separations and immunoblot analyses (chemiluminescence) similar to those samples shown in Fig. 1, lanes E–G. Approximately 150 μg of protein in each gradient fraction was applied to each SDS gel lane. Isolated peroxisomes, identified via catalase activity, were found within fractions 5–13; immuno-reactive AtPex10p was not detected on immunoblots in any of these fractions. AtPex10p was immuno-detected in six fractions (24–29) ranging from 30% to 15% (w/w) Suc, indicating that AtPex10p was associated with structures that migrated out of the applied sample containing 13% (w/w) Suc. Calnexin in ER vesicles also was immunodetected in these six fractions plus others at higher Suc concentrations.

gradient centrifuged in a vertical rotor. Representative results of 10 replicate experiments are shown in Fig. 6. Peroxisomes, identified by catalase activity, equilibrated at a density of approximately 1.25 g/mL, which is the 51% (w/w) region of the gradients. TCA-precipitated proteins in fractions encompassing this region of the gradients (5–13, 59–48% (w/w) Suc) were separated by SDS/PAGE, electroblotted onto Immobilon, and probed with anti-AtPex10p IgGs. The lack of any chemiluminescence detection of any polypeptides in the 43 kD region of this blot is shown in Fig. 6. One concern was that relatively few intact peroxisomes were isolated in a single gradient. Therefore, fractions from the peroxisomal region of six different gradients were pooled, proteins TCA precipitated, and SDS/PAGE products electroblotted. The results were the same as shown in Fig. 6, i.e., no anti-AtPex10p chemiluminescence signal was detected on the blots (data not shown). In summary, AtPex10p was not detected in sucrose-gradient isolated peroxisomes, which confirmed the results from the in vivo epifluorescence experiments (Figs. 2 and 3).

However, AtPex10p was found in fractions 24–29 (about 30–15% (w/w) Suc), which overlapped with the presence of calnexin in these same fractions. Calnexin however, also was present in fractions with higher Suc concentrations that did not possess AtPex10p. The distribution of calnexin was as expected, i.e., at the top of the gradient in fractions of higher Suc concentrations than the applied sample (13% (w/w) Suc) and within the top of the gradient (about 30–38% (w/w) Suc). The extent of calnexin migration into the gradients to about 38% (w/w) Suc was determined in other gradients and is not shown for this gradient. Calnexin characteristically exists within a population of variably ribosome-studded microsomal vesicles that are derived from rough ER during cell homogenization. AtPex10p did not enter the gradient, but migrated out of the applied sample, as did calnexin-bearing rough microsomes. These results indicate that AtPex10p is not a soluble protein, but is bound to structures that equilibrate with low density calnexin-bearing rough microsomes.

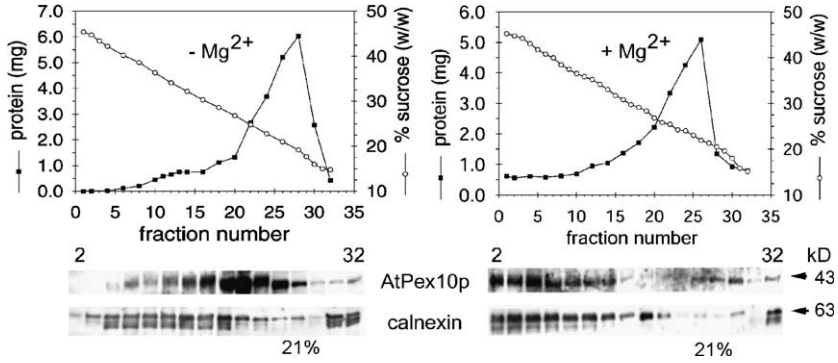

Fig. 7. Microsomal AtPex10p co-fractionates and undergoes a magnesium-induced shift with calnexin to more dense Suc fractions indicative of co-existence of these two proteins in rough ER vesicles. Microsomes (200,000 × *g*, 60 min pellet) isolated from 7-day-old Arabidopsis cells in medium with 5 mM $MgCl_2$ ($+Mg^{2+}$) or with 2 mM EDTA ($-Mg^{2+}$) were layered onto 15–45% (w/w) Suc gradients with or without Mg^{2+}. After centrifugation, proteins in 0.5 mL fractions were deoxycholate solubilized and then TCA precipitated for separations of 150 μg protein in each lane of SDS gels, and subsequent immuno-detection (chemiluminescence) of AtPex10p (43 kD) and calnexin (64 kD) polypeptides electroblotted to Immobilon membranes. The majority of AtPex10p and calnexin migrated to higher Suc concentrations (42–45% Suc, right panel) than when centrifuged in the absence of 5 mM $MgCl_2$ (left panel).

To test this hypothesis, Mg^{2+}-induced shift experiments were done. The presence of Mg^{2+} promotes binding of polyribosomes to microsomal vesicles and thus allows the separation and identification of these vesicles through a characteristic induced shift in equilibrium density within Suc gradients [39,37]. Fig. 7 illustrates results of replicate experiments. In the left panel, AtPex10p- and calnexin-bearing structures migrated out of the applied microsomal pellets (without Mg^{2+}) into the Suc gradient (without Mg^{2+}) and became distributed unevenly throughout most of the entire gradient. Most of the AtPex10p-bearing structures ended up in fractions 16–24 (about 30–22.5% (w/w) Suc). Results illustrated in the right panel wherein the sample and Suc gradient contained Mg^{2+} reveal a distinctly different distribution of AtPex10p- and calnexin-bearing structures within the gradient. That is, both shifted to higher Suc densities (about 42–45% Suc) relative to their distributions in Mg^{2+}-free gradients (left panel).

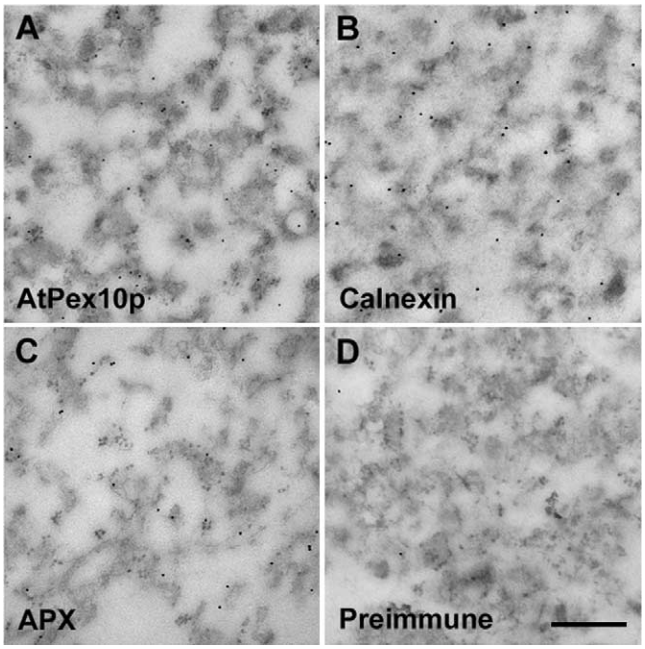

Fig. 8. AtPex10p, calnexin, and ascorbate peroxidase (APX) are localized via electron immunogold microscopy in rough ER vesicles recovered from 42% to 45% Suc fractions (1–5) taken from a Mg^{2+}-containing gradient similar to that illustrated in Fig. 7 (right panel). (A–D) Representative micrographs showing the binding of Protein A–gold particles to primary antibodies applied to thin sections of the pooled gradient samples (fractions 1–5). The material was fixed in glutaraldehyde, but not post-fixed in osmium tetroxide. Gold particles selectively mark antigens in rough ER vesicles (A–C), except when preimmune serum was the applied primary antibody (D). A quantitative assessment of gold particle distribution and frequency over the vesicles (not interim spaces) in these samples is presented in Table 2. Bar = 0.2 μm.

The identity of the Mg^{2+}-shifted structures was investigated via electron immunogold microscopy of the material pooled in fractions 1–5 (Fig. 7, right panel). Fig. 8 is a grouping of electron micrographs illustrating representative results of immunogold analyses with three different antibodies and a preimmune serum control. The pooled material was remarkably uniform in content. It consisted, as expected, of polyribosome-studded membrane vesicles. Gold particles marking the sites of AtPex10p (Fig. 8A) were found predominantly over sectional views of the rough microsomal membranes, rather than over the spaces among the vesicles. The same visual results were obtained with ER calnexin (Fig. 8B) and with peroxisomal ascorbate peroxidase (APX) (Fig. 8C), the latter recently shown to exist in Mg^{2+}-shifted rough ER vesicles [36]. Gold particles were observed infrequently on sections with applied preimmune serum (two particles are visible in Fig. 8D). Table 2 presents comparative statistical data derived from visual counts of gold particles over the microsomal vesicles. Making these counts was feasible because of the uniform nature of the material and because data acquisition was relatively easy to acquire and was reliable. Less than one gold particle per μm^2 was found for the control preimmune sections. The frequency of gold particle binding to

Table 2
Frequency of Protein A-gold particle binding to antigens in thin sections of rough ER vesicles in gradient fractions similar to those shown in Fig. 8

Antigen	Section surface area[a] (particles/μm^2)
AtPex10p	7.9 ± 3.9
AtAPX	14.9 ± 2.9
Calnexin	14.1 ± 3.7
Preimmune serum	0.8 ± 0.3

[a] Mean number of gold particles ± standard deviation.

microsomes was significantly greater for the other three antibody applications, with calnexin and APX IgGs yielding nearly the same frequencies, and AtPex10 IgGs yielding a binding frequency nearly half the others, but well above the background level. The visual data in Fig. 8 coupled with the quantitative assessment of these observations provide strong evidence for the existence of at least some AtPex10p in polyribosome-studded microsomal vesicles derived from cellular rough ER.

These in vitro cell fractionation data collectively confirm interpretations from the in vivo epifluorescence results, i.e., that AtPex10p is present at least in portions (subdomains) of Arabidopsis cell ER, but not in the peroxisomes.

3.6. Topological orientation and membrane association of AtPex10p with rough ER vesicles

Fig. 9 presents the results of various treatments of rough microsomal vesicles employed to assess these features. Panel A, lanes 1 and 2, show that incubation of vesicles exhibiting immuno-detectable AtPex10p, APX, and calnexin (lane A) with Proteinase K (lane 2) results in digestion of AtPex10p and APX, but not calnexin. These results with the positive controls were as expected since APX has been reported to be on the surface of rough ER vesicles and calnexin is mostly within such vesicles [24]. Incubation of vesicles with the protease plus detergent (lane 3), which allows penetration of the protease into intact vesicles, resulted as expected in the digestion of calnexin (and calreticulin, which also was detected with this antibody). This result provides evidence that the vesicles are intact, and that proteins inside of the vesicles are protected from the protease in the absence of detergent. Fig. 9, panel B, shows that the 43 kD AtPex10p in the vesicles (lane 1) is not released in water (lane 2) or 0.2 M KCl (lane 3), but is completely released in alkaline carbonate (lane 4) since none is subsequently found in the detergent-solubilized pellet (lane 5). The interpretation of these data is that AtPex10p is a peripheral membrane protein located mostly on the cytosolic side of the ER membrane.

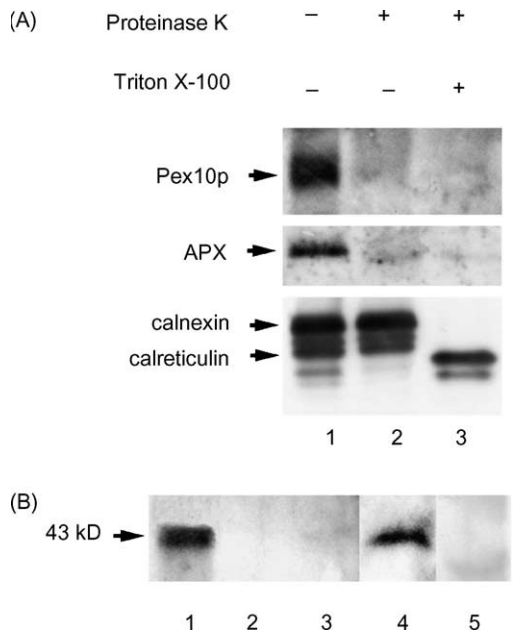

Fig. 9. AtPex10p is interpreted to be a peripherally associated membrane protein located mostly on the cytosolic face of rough ER vesicles. Panels A and B—rough ER vesicles were recovered from 42% to 45% (w/w) region (pooled fractions 1–5) of a $+Mg^{2+}$-containing Suc gradient similar to that represented in Fig. 7 (right panel). Panel A—the vesicles were subjected to Proteinase K digestion (4:1 ratio of vesicle sample protein (1 mg):0.25 mg Proteinase K (5 mg/mL stock solution in water)) in the absence (−) and presence (+) of Triton X-100. Following incubations for 60 min at 4 °C, and addition of 1 mM PMSF to stop the digestion reactions, samples were TCA precipitated for SDS-PAGE (150 μg protein per lane) and chemiluminescence immunoblot analyses. Anti-AtPex10p IgGs recognized a 43 kD polypeptide band and anti-APX and anti-calnexin recognized a 31 and 64 kD band, respectively (lane 1). The calnexin antibody also recognizes calreticulin. Panel B—the vesicles (lane 1, untreated) were sequentially incubated in water (lane 2, supernatant), 0.2 M KCl (lane 3), and alkaline (pH 11.5) sodium carbonate (lane 4) leaving a final pellet, which was incubated in 0.05% deoxycholate to release integral membrane proteins (lane 5). The extracted proteins (in supernatants) were taken to 0.05% deoxycholate, TCA precipitated, and then subjected to SDS-PAGE (150 μg protein per lane) and analyzed on blots (chemiluminescence) with anti-AtPex10p IgGs.

4. Discussion

In the current study we provide evidence from in vivo and vitro experiments that endogenous AtPex10p in suspension-cultured Arabidopsis cells resides in a subdomain of rough ER, but not within peroxisomes. More specifically, the combined data were derived from in vivo immunofluorescence microscopy, immunogold electron microscopy of cells and cell fractions, and biochemical analyses of cell fractions. These findings have important implications in our overall understanding of plant peroxisomal biogenesis, and provide new data relevant to the recent reports describing an At*PEX10* knock out mutant. That is, AtPex10p functions in the ER as a peroxin in Arabidopsis plant cells as surmised by Schumann et al. [62]. We conclude here that AtPex10p is a peroxin homolog as discussed below.

The lack of positive results for the presence of endogenous AtPex10p in peroxisomes was unexpected, yet was consistent among all of our experimental approaches. Immunofluorescence images of non-transformed wild-type cells (Fig. 2) with

anti-AtPex10p IgGs revealed AtPex10p partially colocalized in BiP-containing ER and in unidentified structures observed throughout the non-vacuolar cytoplasm. This non-BiP compartment clearly did not share any colocalizations with catalase-containing peroxisomes (Fig. 2D–I), nor were other plant peroxisomal markers (e.g., APX and PMP73) found without catalase in this region (data not shown). Results from numerous replicate (with diverse variations) and control microscopy experiments confirmed this non-peroxisomal locale, which is discrepant with the localization (but perhaps not the general function) of all other Pex10p homologs. For example, *H. polymorpha* Pex10p (HpPex10p) was localized to the peroxisomal membrane via immunogold microscopy, while the *P. pastoris* (PpPex10p) and human (HsPex10p) Pex10p homologs were localized to peroxisomes via biochemical fractionation and transient expression experiments [28,70]. Others and we have shown previously with Arabidopsis and BY-2 cells that peroxin homologs (e.g., AtPex3p) [26] and PMPs (e.g., APX and PMP22) [36,45,46,48] at steady state and transiently expressed levels are localized to peroxisomes. Hence, using suspension cells as model systems for reliable in vivo and in vitro studies of peroxisomal localization of membrane proteins is well documented. Our cell fractionation/biochemical experiments aimed at characterizing the AtPex10p compartment consistently revealed AtPex10p in a fraction other than peroxisomes (Figs. 6 and 7). Notwithstanding, immunofluorescence microscopy revealed frequent juxtapositions of AtPex10p-labeled structures with peroxisomes, and electron microscopy corroborated close/direct associations of peroxisomes and rough ER (examples shown in Fig. 4).

Several experiments aimed at discerning the localization of AtPex10p (or a fusion thereof) via transient overexpression left us with more questions than answers. For example, we expected that AtPex10p overexpression might lead to at least a partial peroxisomal localization that previously was not observed. Such results would suggest that in addition to an ER localization, part of endogenous AtPex10p normally resides in peroxisomes at a low sometimes undetectable level. Such a result was observed transiently with overexpressed peroxisomal APX, a bona fide PMP [45,44,36,37]. However, transient overexpressions with N- and C-terminal fusions of fluorescent proteins, or with variously epitope-tagged AtPex10p consistently yielded a cytosolic localization of all of the expressed proteins (Fig. 3). In all cases, normal-appearing peroxisomes were present in the transformed cells.

Interestingly, Sparkes et al. [66] reported that overexpressed AtPex10p-YFP sorted in vivo to GFP-SKL-labeled peroxisomes in tobacco epidermal cells. This was interpreted as somewhat indirect evidence for AtPex10p being a plant peroxin homolog, because they or Schumann et al. [62] could not show the localization of AtPex10p in peroxisomes of mutant Arabidopsis embryos. We actually concur with their general interpretation, but continue to be intrigued as to why we have never found evidence for a peroxisomal localization of endogenous AtPex10p, or for transiently expressed AtPex10p fusions, including the very same AtPex10p-YFP that [66] localized in tobacco peroxisomes. As mentioned above with cited references, we and others have localized in several published studies varied endogenous and transiently expressed proteins to peroxisomes in suspension-cultured cells. We have not yet reconciled the differences between our results and those published by Sparkes et al. [66], but offer the following possible three explanations: (1) YFP fusion to AtPex10p results in formation of a cryptic internal peroxisomal targeting signal that is functional in tobacco, but not in Arabidopsis cells; (2) sorting properties of light-grown tobacco leaves and rapidly dividing, dark-grown suspension cultured Arabidopsis cells are different and lead to different localizations of AtPex10p-YFP [41,27]; (3) transient overexpression of AtPex10p fusions in whole plants or suspension-cultured cells is not a reliable means to assess localization of this particular protein. None of these are satisfying, but the results are clearly different in the two plant systems.

At steady state levels, endogenous AtPex10p localized partly to BiP-localized ER (microscopy) as well as to rough ER vesicles classically defined by a Mg^{2+}-shift (Figs. 6–8). The Mg^{2+}-induced shift of calnexin (also shown in Fig. 7) is similar to data shown by others [42,39,36] where vesicles containing calnexin shifted their buoyant density as a function of Mg^{2+}-dependent ribosome attachment. Protein A-gold binding per square micrometer of section area was lower for AtPex10p than for both AtAPX and calnexin in these fractions (Table 2), but the values are reliably greater than the AtPex10p preimmune serum control. Protease plus/minus detergent treatments and solubilization in pH 11 sodium carbonate of rough microsomal vesicles revealed that AtPex10p is a rather tightly associated peripheral membrane protein residing mostly on the cytosolic side of the ER membrane (Fig. 9). The peripheral membrane association of AtPex10p was not expected due to the two computer-predicted transmembrane domains [62]. However, such hydrophobic domains can also reflect hydrophobic interiors of a globular protein, or in this case, the interior of a peripheral membrane protein. HpPex10p and PpPex10p were reported to be resistant to alkaline sodium carbonate extraction, and consequently were interpreted to be integral PMPs [28,70]. This response with AtPex10p is analogous to the unexpected sodium carbonate extraction observed with the ER-localized portion of the tail-anchored membrane protein APX [36] and may represent a feature unique to plant peroxins.

The combined unequivocal Mg^{2+}-induced shift, immunogold ultrastructural localization of AtPex10p to rough ER vesicles (Figs. 7 and 8) and the ER-vesicle peripheral association and topology (Fig. 9) are compelling collective evidences for the localization and function of AtPex10p in Arabidopsis ER. Additional support for the residence of AtPex10p in ER comes from another study as well. Utilizing

a bioinformatics approach to identify Arabidopsis proteins conforming to a novel C-terminal ER retrieval motif that was identified first on Δ^{12} fatty acid desaturase proteins, McCartney et al. [43] identified 47 proteins containing the Φ-X-X-K/R/D/E-Φ-COOH consensus sequence, where Φ are large hydrophobic amino acid residues. Remarkably, the C-terminus of AtPex10p conforms to this motif, and fusion of the C-terminal AtPex10p sequence (-YHSDF) to the reporter protein GFP-LAMP1-G resulted in localization to the ER membrane [43] The identification of AtPex10p as the only putative plant peroxin with this signal sequence also suggests a localization and function different from other Pex10p homologs.

The nuances of Pex10p function reported in other systems may not a priori require a static localization of AtPex10p in peroxisomes. A feature consistent with the various Pex10p homologs is that cells void of functional Pex10p are severely compromised. Often the import of matrix proteins is impaired, with many Pex10p mutants displaying radically altered cellular morphologies, e.g., swollen ER strands (ΔAt*PEX10*), bizarre membranous structures (ΔPp*PEX10* and ΔAt*PEX10*), peroxisomal ghosts (ΔHp*PEX10*), or no identifiable peroxisomes at all (ΔPp*PEX10*, ΔHp*PEX10* and ΔAt*PEX10*); these most often lead to lethality or conditional survival. In the case of the AtPex10p-deficient Arabidopsis mutant analyzed previously [62], the import competency of peroxisomes could not be analyzed because these organelles apparently were not present in the cells. It remains to be determined whether the absence of AtPex10p in this T-DNA mutant is the cause of lethality or simply an effector perturbing another yet unknown factor. The development of a conditionally lethal AtPEX10 mutant or investigations into the localization of AtPex10p in T-DNA mutants of other Arabidopsis proteins shown to interact with Pex10p in other systems (such as Pex2p, Pex12p or Pex4p) may answer such a question. However, there is mounting evidence in most organisms examined, that Pex10p is intricately involved in the dynamic segregation and trafficking of vesicular or membrane-associated cargo between organelles such as vacuoles, lipid bodies, protein bodies, ER and/or peroxisomes (Chang et al., 1999a; [62,70]). As shown in this study, AtPex10p resides in a subdomain of rough ER. It is not clear whether this subdomain is the same as the peroxisomal ER (pER) subdomain that was identified by the localization of peroxisomal APX [36,37,45]. An immunofluorescence comparison of the localizations of endogenous AtPex10p and APX was unreliable because polyclonal antibodies to both proteins were from the same animal host. Although cell fractionation experiments revealed both proteins in the same ER fractions, the analyses did not permit discrimination of specific subdomains. If they are not in the same subdomain, then we would not consider AtPex10p as a pER resident protein. Our rationale is that an authentic pER resident protein must colocalize, at least partially, with another bona fide peroxisomal protein. Until such a colocalization can be demonstrated for AtPex10p, this denotation should be reserved. However, AtPex10p may serve as part of a highly organized, yet unknown, ER fidelity mechanism that specifically discriminates for proteins, lipids and/or metabolite components destined for peroxisomes.

Taken as a whole, our findings regarding AtPex10p localization do not reveal a function for this putative Arabidopsis Pex10p homolog. However, our assignment of AtPex10p to a rough ER subdomain limits its suspected involvement in plant peroxisomal biogenesis. Peroxins initially were defined by Distel et al. [15] as proteins involved in the formation, division, or degradation of peroxisomes, either directly through *cis* acting factors present in peroxisomes, or indirectly via formation of other components required for such processes (e.g., membranes, protein import complexes, etc.). In non-plant organisms such as yeast and mammals, peroxins often are easily identified by partial or conditional functions such as the ability to rescue peroxisomal-deficient phenotypes (mammals) or the restoration of an ability to grow on oleate or other carbon sources (yeasts). With plants, these types of experiments are difficult to carry out and to date, have only been done in a reverse fashion by partially complementing yeast *PEX* knockouts with Arabidopsis genes (e.g. *AtPEX10* [62]; *AtPEX16* [35]). Because of these limitations, other techniques and definitions may be required for establishing putative proteins as bona fide plant peroxins. Our findings represent the first localization of a plant peroxin homolog to the ER, and coupled with the data from others (for review and more comments see [65,74]), suggest an early biogenetic role for AtPex10p as a peroxin in plant peroxisome formation, perhaps in partitioning other proteins or lipids destined for peroxisomes from ER.

Acknowledgements

Steven Neill (University of West England, Bristol, UK) is gratefully acknowledged for providing the Arabidopsis suspension cells. Special thanks are due those colleagues, listed in Section 3, who donated antibodies used in this research. Daisy Savarirajan maintained the Arabidopsis cell cultures during a portion of this study. The electron microscopy was done in the ASU Life Sciences Electron Microscopy Facility. Sincere thanks are extended to Dr. Cayle Lisenbee for his numerous discussions on the interpretations of our data, guidance and help with the cell fractionation methods and immunogold microscopy, and his encouragement to several members of the research team. Mrs. Sheetal Karnik and Mrs. Joanne Hunt are thanked for their many thoughtful discussions, and help with the epifluorescence microscopy. We are grateful to Dr. Scott Bingham for his expert advice and key suggestions related to plasmid constructions, DNA sequencing, and general recombinant DNA procedures. Dr. Robert Roberson made important contributions by providing formvar-coated grids

and gold-reflecting cell sections, and advice on immunogold labeling. A special thanks is extended to Matthew Lingard for his preparation of the CAMBIA/AtPEX10-YFP (gift from I. Sparkes), biolistic bombardment of Arabidopisis and BY-2 cells, and photographed images of some transformed cells. We also thank Dr. Robert Mullen (University of Guelph) for several insightful discussions and for preparing the pRTL2ΔNS *Xba*I–*Bam*HI–*myc* construct.

References

[1] R. Baerends, S. Rasmussen, R. Hilbrands, Mvd. Heide, K. Faber, P. Reuvekamp, J. Kiel, J. Cregg, Ivd. Klei, M. Veenhuis, The *Hansenula polymorpha* PER9 gene encodes a peroxisomal membrane protein essential for peroxisome assembly and integrity, J. Biol. Chem. 271 (1996) 8887–8894.

[2] R. Bascom, H. Chan, R. Rachubinski, Peroxisome biogenesis occurs in an unsynchronized manner in close association with the endoplasmic reticulum in temperature-sensitive *Yarrowia lipolytica* Pex3p mutants, Mol. Biol. Cell 14 (2003) 939–957.

[3] J. Bunkelmann, R. Trelease, Ascorbate peroxidase. A prominent membrane protein in oilseed glyoxysomes, Plant Physiol. 110 (1996) 589–598.

[4] C. Chang, S. South, D. Warren, J. Jones, A. Moser, S. Gould, Metabolic control of peroxisome abundance, J. Cell Sci. (1999a) 1579–1590.

[5] C. Chang, D. Warren, K. Sacksteder, S. Gould, PEX12 interacts with PEX5 and PEX10 and acts downstream of receptor docking in peroxisomal matrix protein import, J. Cell Biol. 147 (1999) 761–774.

[6] W. Charlton, E. Lopez-Huertas, PEX genes in plants and other organisms, in: A. Baker, I. Graham (Eds.), Plant Peroxisomes: Biochemistry, Cell Biology and Biotechnological Applications, Kluwer Academic Publishers, The Netherlands, 2002, pp. 385–426.

[7] Z. Chen, J. Ticigliano, D. Klessig, Purification and characterization of a soluble salicylic acid-binding protein from tobacco, Proc. Natt. Acad. Sci. USA (1993) 9533–9537.

[8] J. Cornah, S. Smith, Synthesis and function of glyoxylate cycle enzymes, in: A. Baker, I. Graham (Eds.), Plant Peroxisomes: Biochemistry, Cell Biology and Biotechnological Applications, Kluwer Academic Publishers, Dordecht, 2002, pp. 57–101.

[9] F. Corpas, J. Barroso, L. Rio, Peroxisomes as a source of reactive oxygen species and nitric oxide signal molecules in plant cells, Trends Plant Sci. 6 (2001) 145–150.

[10] F. Corpas, J. Bunkelmann, R. Trelease, Identification and immunochemical characterization of a family of peroxisome membrane proteins (PMPs) in oilseed glyoxysomes, Eur. J. Cell Biol. 65 (1994) 280–290.

[11] S. Coughlan, C. Hastings, R. Winfrey, Cloning and characterization of the calreticulin gene from *Ricinus communis* L., Plant Mol. Biol. 34 (1997) 897–911.

[12] L. del Rio, F. Corpas, L. Sandalio, J. Palma, M. Gomez, J. Barroso, Reactive oxygen species, antioxidant systems and nitric oxide in peroxisomes, J. Exp. Bot. 53 (2002) 1255–1272.

[13] L. del Rio, L. Sandalio, J. Palma, F. Corpas, E. Lopez-Huertas, M. Romero-Puertas, I. McCarthy, Peroxisomes, reactive oxygen metabolism, and stress-related enzyme activities, in: A. Baker, I. Graham (Eds.), Plant Peroxisomes: Biochemistry, Cell Biology and Biotechnological Applications, Kluwer Academic Publishers, The Netherlands, 2002, pp. 221–258.

[14] K. Dhugga, S. Tiwari, P. Ray, A reversibly glycosylated polypeptide (RGP1) possibly involved in plant cell wall synthesis: purification, gene cloning, and trans-Golgi localization, Proc. Natl. Acad. Sci. U.S.A. 94 (1997) 7679–7684.

[15] B. Distel, R. Erdmann, S. Gould, G. Blobel, D. Crane, J. Cregg, G. Dodt, Y. Fujiki, J. Goodman, W. Just, J. Kiel, W. Kunau, P. Lazarow, G. Mannaerts, H. Moser, T. Osumi, R. Rachubinski, S. Roscher, S. Subramani, H. Tabak, T. Tsukamoto, D. Valle, Ivd. Klei, Pv. Veldhoven, M. Veenhuis, A unified nomenclature for peroxisome biogenesis factors, J. Cell Biol. 135 (1996) 1–3.

[16] J. Dyer, J. McNew, J. Goodman, The sorting sequence of the peroxisomal integral membrane protein PMP47 is contained within a short hydrophilic loop, J. Cell Biol. 133 (1996) 269–280.

[17] G. Eitzen, R. Szilard, R. Rachubinski, Enlarged peroxisomes are present in oleic acid-grown *Yarrowia lipolytica* overexpressing the PEX16 gene encoding an intraperoxisomal peripheral membrane peroxin, J. Cell Biol. 137 (1997) 1265–1278.

[18] O. Emanuelsson, A. Elofsson, G. Heijne, S. Cristobal, In silico prediction of the peroxisomal proteome in fungi, plants and animals, J. Mol. Biol. 330 (2003) 443–456.

[19] K. Faber, R. Dijk, I. Keizer-Gunnink, A. Koek, I. Klei, M. Veenhuis, Import of assembled PTS1 proteins into peroxisomes of the yeast *Hansenula polymorpha*: yes and no! Biochim. Biophys. Acta 1591 (2002) 157–162.

[20] C.R. Flynn, R. Mullen, R. Trelease, Mutational analyses of a type 2 peroxisomal targeting signal that is capable of directing oligomeric protein import into tobacco BY-2 glyoxysomes, Plant J. 16 (1998) 709–720.

[21] Y. Fujiki, K. Okumoto, H. Otera, S. Tamura, Peroxisome biogenesis and molecular defects in peroxisome assembly disorders, Cell Biochem. Biophys. 32 (2000) 155–164.

[22] H. Geuze, J. Murk, A. Stroobants, J. Griffith, M. Kleijmeer, A. Koster, A. Verkleij, B. Distel, H. Tabak, Involvement of the endoplasmic reticulum in peroxisome formation, Mol. Biol. Cell 14 (2003) 2900–2907.

[23] J. Haseloff, K. Siemering, D. Prasher, S. Hodge, Removal of a cryptic intron and subcellular localization of green fluorescent protein are required to mark transgenic Arabidopsis plants brightly, Proc. Natl. Acad. Sci. U.S.A. 94 (1997) 2122–2127.

[24] L. Huang, A. Franklin, N. Hoffman, Primary structure and characterization of an Arabidopsis thaliana colnexin-like protein, J. Biol. Chem. (1993) 6560–6566.

[25] A. Huang, R. Trelease, T. Moore, Plant Peroxisomes, Academic Press, New York, 1983.

[26] J. Hunt, R. Trelease, Sorting pathway and molecular targeting signals for the Arabidopsis peroxin 3, Biochem. Biophys. Res. Commun. 314 (2004) 589–596.

[27] G. Jedd, N.-H. Chua, Visualization of peroxisomes in living plant cells reveals acto-myosin-dependent cytoplasmic streaming and peroxisome budding, Plant Cell Physiol. 43 (2002) 384–392.

[28] J. Kalish, C. Theda, J. Morrell, J. Berg, S. Gould, Formation of the peroxisome lumen is abolished by loss of *Pichia pastoris* Pas7p, a zinc-binding integral membrane protein of the peroxisome, Mol. Cell Biol. 15 (1995) 6406–6419.

[29] T. Kamada, K. Nito, H. Hayashi, S. Mano, M. Hayashi, M. Nishimura, Functional differentiation of peroxisomes revealed by expression profiles of peroxisomal genes in *Arabidopsis thaliana*, Plant Cell Physiol. 44 (2003) 1275–1289.

[30] W. Kunau, R. Erdmann, Peroxisome biogenesis: back to the endoplasmic reticulum? Curr. Biol. 8 (1998) 9R209–9R302.

[31] C. Kunce, R. Trelease, R. Turley, Purification and biosynthesis of cottonseed (*Gossypium hirsutum* L.) catalase, Biochem. J. 251 (1988) 147–155.

[32] P. Lazarow, Peroxisome biogenesis: advances and conundrums, Curr. Opin. Cell Biol. 15 (2003) 489–497.

[33] P. Lazarow, Y. Fujiki, Biogenesis of peroxisomes, Annu. Rev. Cell Biol. 1 (1985) 489–530.

[34] M. Lee, R. Mullen, R. Trelease, Oilseed isocitrate lyases lacking their essential type 1 peroxisomal targeting signal are piggybacked to glyoxysomes, Plant Cell 9 (1997) 185–197.

[35] Y. Lin, L. Sun, L. Nguyen, R. Rachubinski, H. Goodman, The Pex16p homolog SSE1 and storage organelle formation in Arabidopsis seeds, Science 284 (1999) 328–330.
[36] C. Lisenbee, M. Heinze, R. Trelease, Peroxisomal ascorbate peroxidase resides within a subdomain of rough endoplasmic reticulum in wild-type Arabidopsis cells, Plant Physiol. 132 (2003) 870–882.
[37] C. Lisenbee, S. Karnik, R. Trelease, Overexpression and mislocalization of a tail-anchored GFP redefines the identity of peroxisomal ER, Traffic 4 (2003) 491–501.
[38] E. Lopez-Huertas, W. Charlton, B. Johnson, I. Graham, A. Baker, Stress induces peroxisome biogenesis genes, EMBO J. 19 (2000) 6770–6777.
[39] S. Lu, E. Hrabak, An Arabidopsis calcium-dependent protein kinase is associated with the endoplasmic reticulum, Plant Physiol. 128 (2002) 1008–1021.
[40] M. Luethy, A. Horak, T. Elthon, Monoclonal antibodies to the [alpha]- and [beta]-subunits of the plant mitochondrial F1-ATPase, Plant Physiol. 101 (1993) 931–937.
[41] J. Mathur, N. Mathur, M. Hulskamp, Simultaneous visualization of peroxisomes and cytoskeletal elements reveals actin and not microtubule-based peroxisome motility in plants, Plant Physiol. 128 (2002) 1031–1045.
[42] K. Matsuoka, T. Higuchi, M. Maeshima, K. Nakamura, A vacuolar-type H+-ATPase in a nonvacuolar organelle is required for the sorting of soluble vacuolar protein precursors in tobacco cells, Plant Cell 9 (1997) 533–546.
[43] A. McCartney, J. Dyer, P. Dhanoa, P. Kim, D. Andrews, J. McNew, R. Mullen, Membrane-bound fatty acid desaturases are inserted co-translationally into the ER and contain different ER retrieval motifs at their carboxy termini, Plant J. 37 (2004) 156–173.
[44] R. Mullen, C. Lisenbee, C.R. Flynn, R. Trelease, Stable and transient expression of chimeric peroxisomal membrane proteins induces an independent ''zippering'' of peroxisomes and an endoplasmic reticulum subdomain, Planta 213 (2001) 849–863.
[45] R. Mullen, C. Lisenbee, J. Miernyk, R. Trelease, Peroxisomal membrane ascorbate peroxidase is sorted to a membranous network that resembles a subdomain of the endoplasmic reticulum, Plant Cell 11 (1999) 2167–2185.
[46] R. Mullen, R. Trelease, Biogenesis and membrane properties of perixosmes: does the boundary membrane serve and protect, Trends Plant Sci. 1 (1996) 363–402.
[47] R. Mullen, R. Trelease, The sorting signals for peroxisomal membrane-bound ascorbate peroxidase are within its C-terminal tail, J. Biol. Chem. 275 (2000) 16337–16344.
[48] M. Murphy, B. Phillipson, A. Baker, R. Mullen, Characterization of the targeting signal of the Arabidopsis 22 kD integral peroxisomal membrane protein, Plant Physiol. 133 (2003) 813–828.
[49] T. Nakamura, S. Yokota, Y. Muramoto, K. Tsutsui, Y. Oguri, K. Fukui, T. Takabe, Expression of a betaine aldehyde dehydrogenase gene in rice, a glycinebetaine nonaccumulator, and possible localization of its protein in peroxisomes, Plant J. 11 (1997) 1115–1120.
[50] E. Newcomb, Y. Kaneko, K. Van den Bosch, Specialization of the inner cortex for ureide production in soybean root nodules, Protoplasma 150 (1989) 150–159.
[51] M. Nishimura, M. Hayashi, A. Kato, K. Yamaguchi, S. Mano, Functional transformation of microbodies in higher plant cells, Cell Struct. Funct. 21 (1996) 387–393.
[52] K. Okumoto, I. Abe, Y. Fujiki, Molecular anatomy of the peroxin Pex12p: ring finger domain is essential for Pex12p function and interacts with the peroxisome-targeting signal type 1-receptor Pex5p and a ring peroxin, Pex10p, J. Biol. Chem. 275 (2000) 25700–25710.
[53] K. Okumoto, R. Itoh, N. Shimozawa, Y. Suzuki, S. Tamura, N. Kondo, Y. Fujiki, Mutations in PEX10 is the cause of Zellweger peroxisome deficiency syndrome of complementation group B, Hum. Mol. Genet. 7 (1998) 1399–1405.
[54] L. Olsen, J. Harada, Peroxisomes and their assembly in higher plants, Ann. Rev. Plant Physiol. Plant Mol. Biol. 46 (1995) 123–146.
[55] J. Palma, L. Sandalio, F. Corpas, M. Romero-Puertas, I. McCarthy, L. Rio, Plant proteases, protein degradation, and oxidative stress: role of peroxisomes, Plant Physiol. Biochem. 40 (2002) 521–530.
[56] S. Reumann, The structural properties of plant peroxisomes and their metabolic significance, Biol. Chem. 381 (2000) 639–648.
[57] S. Reumann, The photorespiratory pathway of leaf peroxisomes, in: A. Baker, I. Graham (Eds.), Plant Peroxisomes: Biochemistry, Cell Biology and Biotechnological Applications, Kluwer Academic Publishers, The Netherlands, 2002, pp. 141–189.
[58] R. Sabba, N. Durso, K. Vaughn, Structural and immunocytochemical characterization of the walls of dichlobenil-habituated BY-2 tobacco cells, Int. J. Plant Sci. 160 (1999) 275–290.
[59] F. Salomons, I. Klei, A. Kram, W. Harder, M. Veenhuis, Brefeldin A interferes with peroxisomal protein sorting in the yeast *Hansenula polymorpha*, FEBS Lett. 411 (1997) 133–139.
[60] P. Sanders, P. Lee, C. Biesgen, J. Boone, T. Beals, E. Weiler, R. Goldberg, The Arabidopsis DELAYED DEHISCENCE1 gene encodes an enzyme in the jasmonic acid synthesis pathway, Plant Cell 12 (2000) 1041–1061.
[61] U. Schumann, C. Gietl, M. Schmid, Sequence analysis of a cDNA encoding Pex10p, a zinc-binding peroxisomal integral membrane protein from *Arabidopsis thaliana* (Accession No. AF119572), Plant Physiol. 119 (1999) 1147.
[62] U. Schumann, G. Wanner, M. Veenhuis, M. Schmid, C. Gietl, Ath-PEX10, a nuclear gene essential for peroxisome and storage organelle formation during Arabidopsis embryogenesis, Proc. Natl. Acad. Sci. U.S.A. 100 (2003) 9626–9631.
[63] W. Snyder, K. Faber, T. Wenzel, A. Koller, G. Luers, L. Rangell, G. Keller, S. Subramani, Pex19p interacts with Pex3p and Pex10p and is essential for peroxisome biogenesis in *Pichia pastoris*, Mol. Biol. Cell 10 (1999) 1745–1761.
[64] S. South, E. Baumgart, S. Gould, Inactivation of the endoplasmic reticulum protein translocation factor, Sec61p, or its homolog, Ssh1p, does not affect peroxisome biogenesis, Proc. Natl. Acad. Sci. U.S.A. 98 (2001) 12027–12031.
[65] I. Sparkes, A. Baker, Peroxisome biogenesis and protein import in plants, animals and yeasts: enigma and variations? (Review) Mol. Membr. Biol. (2002) 171–185.
[66] I. Sparkes, F. Brandizzi, S. Slocombe, M. El-Shami, C. Hawes, A. Baker, An Arabidopsis pex10 null mutant is embryo lethal, implicating peroxisomes in an essential role during plant embryogenesis, Plant Physiol. 133 (2003) 1809–1819.
[67] A. Stintz, J. Browse, The Arabidopsis male-sterile mutant, opr3, lacks the 12-oxophytodienoic acid reductase required for jasmonate synthesis, Proc. Natl. Acad. Sci. U.S.A. 97 (2000) 10625–10630.
[68] S. Subramani, Components involved in peroxisome import, biogenesis, proliferation, turnover, and movement, Physiol. Rev. 78 (1998) 171–188.
[69] H. Tabak, J. Murk, I. Braakman, H. Geuze, Peroxisomes start their life in the endoplasmic reticulum, Traffic 4 (2003) 512–518.
[70] X. Tan, H. Waterham, M. Veenhuis, J. Cregg, The *Hansenula polymorpha* PER8 gene encodes a novel peroxisomal integral membrane protein involved in proliferation, J. Cell Biol. 128 (1995) 307–319.
[71] V. Titorenko, D. Ogrydziak, R. Rachubinski, Four distinct secretory pathways serve protein secretion, cell surface growth, and peroxisome biogenesis in the yeast *Yarrowia lipolytica*, Mol. Cell Biol. 17 (1997) 5210–5226.
[72] V. Titorenko, R. Rachubinski, Dynamics of peroxisome assembly and function, Trends Cell Biol. 11 (2001) 22–29.
[73] V. Titorenko, R. Rachubinski, The peroxisome: orchestrating important developmental decisions from inside the cell, J. Cell Biol. 164 (2004) 641–645.
[74] R. Trelease, Peroxisomal biogenesis and acquisition of membrane proteins, in: A. Baker, I. Graham (Eds.), Plant Peroxisomes: Biochemisty, Cell Biology and Biotechnological Applications, Kluwer Academic Publishers, Dordecht, The Netherlands, 2002 pp. 305–337.

[75] D. Verma, Peroxisome biogenesis in root nodules and assimilation of symbiotically reduced nitrogen in tropical legumes, in: A. Baker, I. Graham (Eds.), Plant Peroxisomes: Biochemistry, Cell Biology and Biotechnological Applications, Kluwer Academic Publishers, The Netherlands, 2002, pp. 191–220.

[76] F. Vizeacoumar, J. Torres-Guzman, D. Bouard, J. Aitchison, R. Rachubinski, Pex30p, Pex31p, and Pex32p form a family of peroxisomal integral membrane proteins regulating peroxisome size and number in *Saccharomyces cerevisiae*, Mol. Biol. Cell 15 (2004) 665–677.

[77] D. Warren, J. Morrell, H. Moser, D. Valle, S. Gould, Identification of PEX10, the gene defective in complementation group 7 of the peroxisome-biogenesis disorders, Am. J. Hum. Genet. 63 (1998) 347–359.

[78] B. Zolman, I. Silva, B. Bartel, The Arabidopsis pxa1 mutant is defective in an ATP-binding cassette transporter-like protein required for peroxisomal fatty acid beta-oxidation, Plant Physiol. 127 (2001) 1266–1278.